Cell Genomics

Article

Long genetic and social isolation in Neanderthals before their extinction

Graphical abstract

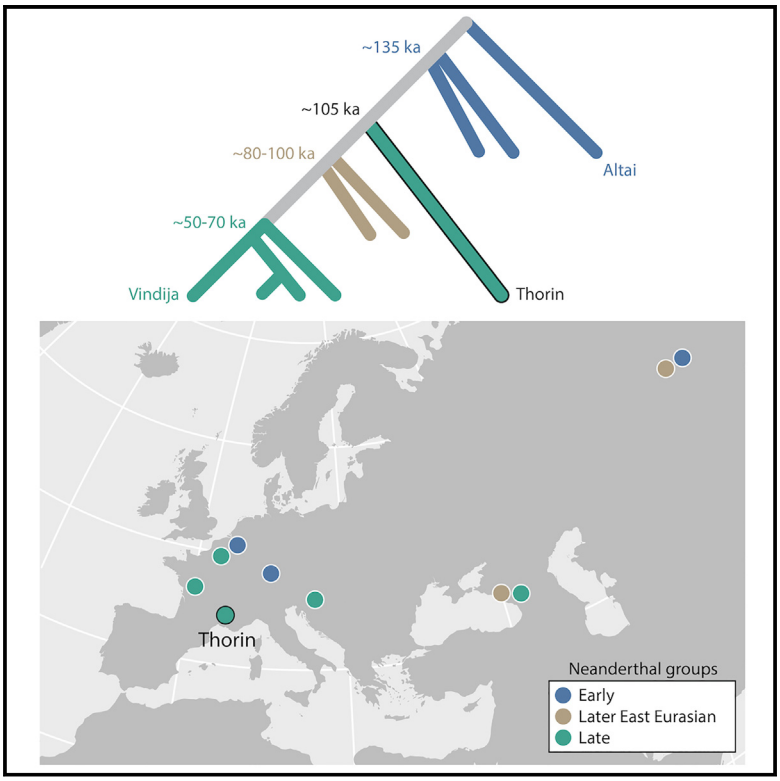

Highlights

- We present the discovery of a Neanderthal body and its genome
- It is one of the last representatives of these populations in Eurasia
- It belongs to an unknown lineage, isolated for 50 ka
- It is similar to Gibraltar Neanderthals, with whom it forms a specific branch

Authors

Ludovic Slimak, Tharsika Vimala, Andaine Seguin-Orlando, ..., Olivier Dutour, Thomas Higham, Martin Sikora

Correspondence

ludovic.slimak@cnrs.fr (L.S.), martin.sikora@sund.ku.dk (M.S.)

In brief

Slimak et al. report the discovery of a late Neanderthal individual from Grotte Mandrin in Mediterranean France and its genome. The genome reveals a relatively early divergence at ~100,000 years ago with other late Neanderthals. It belonged to a population with a small group size that showed no introgression with other known late European Neanderthals, revealing ~50 ka of genetic isolation. These results have important implications for resolving competing hypotheses about the causes of the disappearance of the Neanderthals.

Slimak et al., 2024, Cell Genomics *4*, 100593
September 11, 2024
https://doi.org/10.1016/j.xgen.2024.100593

CellPress

Cell Genomics

CellPress
OPEN ACCESS

Article

Long genetic and social isolation in Neanderthals before their extinction

Ludovic Slimak,[1,22,*] Tharsika Vimala,[2,22] Andaine Seguin-Orlando,[1,2,22,23] Laure Metz,[3,4] Clément Zanolli,[5] Renaud Joannes-Boyau,[6] Marine Frouin,[7,8] Lee J. Arnold,[9] Martina Demuro,[9] Thibaut Devièse,[10] Daniel Comeskey,[11] Michael Buckley,[12] Hubert Camus,[13] Xavier Muth,[14] Jason E. Lewis,[8,15] Hervé Bocherens,[16] Pascale Yvorra,[3] Christophe Tenailleau,[17] Benjamin Duployer,[17] Hélène Coqueugniot,[18,21] Olivier Dutour,[18,21] Thomas Higham,[19,20] and Martin Sikora[2,24,*]

[1]Centre d'Anthropobiologie et de Génomique de Toulouse (CNRS UMR 5288), Université Paul Sabatier, Faculté de Santé, Bâtiment A, 37 allées Jules Guesde, 31000 Toulouse, France
[2]Lundbeck Foundation GeoGenetics Center, University of Copenhagen, 1350K Copenhagen, Denmark
[3]Aix-Marseille Université, CNRS, Min. Culture, UMR 7269, LAMPEA, Maison Méditerranéenne des Sciences de l'Homme, BP 647, 5 rue du Château de l'Horloge, 13094 Aix-en-Provence Cedex 2, France
[4]University of Connecticut, College of Liberal Arts and Sciences, 215 Glenbrook Road, U-4098, Storrs, CT 06269-4098, USA
[5]Univ. Bordeaux, CNRS, MCC, PACEA, UMR 5199, 33600 Pessac, France
[6]Geoarchaeology & Archaeometry Research Group (GARG), Southern Cross University, Military Rd., Lismore, NSW 2480, Australia
[7]Department of Geosciences, Stony Brook University, 255 Earth and Space Sciences Building, Stony Brook, NY 11794-2100, USA
[8]Turkana Basin Institute, Stony Brook University, Stony Brook, NY 11794-4364, USA
[9]School of Physical Sciences, Environment Institute, Institute for Photonics and Advanced Sensing (IPAS), University of Adelaide, North Terrace Campus, Adelaide, SA 5005, Australia
[10]CEREGE, Aix-Marseille University, CNRS, IRD, INRAE, Collège de France, Technopôle de l'Arbois, Aix-en-Provence, France
[11]Syft Technologies Ltd., 3 Craft Place, Middleton, PO Box 28 149, Christchurch 8242, New Zealand
[12]Department of Earth and Environmental Sciences, Manchester Institute of Biotechnology, University of Manchester, Manchester, UK
[13]PROTEE-EXPERT, 4 rue des Aspholdèles, 34750 Villeneuve-lès-Maguelone, France
[14]Get in Situ, 1091 Bourg-en-Lavaux, Switzerland
[15]Chronicle Heritage, 319 E Palm Lane, Phoenix, AZ 85004, USA
[16]Fachbereich Geowissenschaften Forschungsbereich Paläobiologie - Biogeologie Senckenberg, Centre for Human Evolution and Palaeoenvironment (SHEP), Universität Tübingen, Hölderlinstr. 12, 72074 Tübingen, Germany
[17]Centre Inter-Universitaire de Recherche et d'Ingénierie des Matériaux, UMR 5085 CNRS-Université de Toulouse (Paul Sabatier), 118 route de Narbonne, 31062 Toulouse Cedex 9, France
[18]École Pratique des Hautes Études - Paris Sciences et Lettres University, 4-14 rue Ferrus, 75014 Paris, France
[19]Department of Evolutionary Anthropology, Faculty of Life Sciences, University of Vienna, Djerassiplatz 1, 1030 Vienna, Austria
[20]Human Evolution and Archaeological Sciences Forschungsverbund, University of Vienna, Vienna 1090, Austria
[21]University of Bordeaux-Montaigne, CNRS, EPHE, Archéosciences, UMR 6034, 33607 Pessac, France
[22]These authors contributed equally
[23]Present address: Centre d'Anthropobiologie et de Génomique de Toulouse (CNRS UMR 5288), Université Paul Sabatier, Faculté de Santé, Bâtiment A, 37 allées Jules Guesde, 31000 Toulouse, France
[24]Lead contact
*Correspondence: ludovic.slimak@cnrs.fr (L.S.), martin.sikora@sund.ku.dk (M.S.)
https://doi.org/10.1016/j.xgen.2024.100593

SUMMARY

Neanderthal genomes have been recovered from sites across Eurasia, painting an increasingly complex picture of their populations' structure that mostly indicates that late European Neanderthals belonged to a single metapopulation with no significant evidence of population structure. Here, we report the discovery of a late Neanderthal individual, nicknamed "Thorin," from Grotte Mandrin in Mediterranean France, and his genome. These dentognathic fossils, including a rare example of distomolars, are associated with a rich archeological record of Neanderthal final technological traditions in this region ~50–42 thousand years ago. Thorin's genome reveals a relatively early divergence of ~105 ka with other late Neanderthals. Thorin belonged to a population with a small group size that showed no genetic introgression with other known late European Neanderthals, revealing some 50 ka of genetic isolation of his lineage despite them living in neighboring regions. These results have important implications for resolving competing hypotheses about causes of the disappearance of the Neanderthals.

INTRODUCTION

Multiple theories have been presented over the years to address the Neanderthals' extinction ~40 thousand years ago. These approaches are commonly based on the identification of various incidents, ranging from climatic changes to volcanic eruptions or magnetic field reversals. They are thus attributed to ecological factors, implying that the Neanderthals' extinction was more the result of natural events of external origin rather than of processes related to the biological and cultural features of these populations themselves. Internal causes, based on the social, historical, or ethological structures of Neanderthal populations, remain largely underexplored.[1–7] It should be noted that paleogenomic and osteological studies have revealed low effective population sizes and signatures of inbreeding in Siberian and late European Neanderthals,[7–9] suggesting social structures characterized by small group sizes and low intergroup mobility. This contrasts with recent results from early Eurasian modern humans, which showed low levels of inbreeding and higher intergroup mobility despite small group sizes.[9,10] Whether these results are representative of wider Neanderthal and modern human social organization remains inconclusive.

Since the publication of the first draft of the Neanderthal genome in 2010,[11] Neanderthal genomes have been recovered from sites across Eurasia, painting an increasingly complex picture of Neanderthal genetic structure. The deepest divergence among Neanderthal genomes sequenced to date is found between eastern and western Eurasian Neanderthal populations represented by the ~120 kiloannum (ka) Altai Neanderthal from Denisova Cave[8] and the >44 ka Vindija 33.19 individual from Croatia.[12] Genomic data of all other available Neanderthal remains, the earliest in western Europe being ~120 ka (Scladina and Hohlenstein-Stadel [HST]), while the latest being ~40 ka, suggest genetic continuity in western Eurasia for ~80 ka.[13] Recent results obtained from sedimentary DNA suggest that the genetic landscape was significantly altered by expansions of Neanderthal populations ~105 ka.[14] This gave rise to lineages in Europe represented by samples from central Europe (Vindija), the Caucasus (Mezmaiskaya Cave), and Siberia (Chagyrskaya Cave 8),[15] the latter likely replacing the earlier Altai-like population. The genomes of late (<50 ka) European Neanderthals, including an individual from the Caucasus (Mezmaiskaya 2), were found to be more similar to Vindija than to other known lineages, indicating further population turnover toward the last stages of Neanderthal history in the Caucasus or western Europe.[16] The close correlation between genetic similarities and geographic location suggested an absence of major population structure among the sampled late Neanderthal populations. It remains unknown whether these patterns result from long-term *in situ* evolution of late European Neanderthal populations or as a consequence of a recent expansion of Vindija-like lineages into Europe.

Here, we report the discovery of a late Neanderthal individual, nicknamed "Thorin," in 2015, and progressively excavated since then at Grotte Mandrin in Mediterranean France, a site that also was temporarily occupied by early modern humans at 54 ka.[1] Thorin is one of the best-represented Neanderthal individuals found in France since the discovery from Saint-Césaire in 1979.[17] Combining archaeological, chronostratigraphic, isotopic, and genomic analyses, we show that Thorin belonged to a late Neanderthal population that had stayed genetically isolated for ~50 ka. Separate from the Thorin lineage, we find evidence of gene flow from another lineage, which diverged from the ancestral lineage of the European Neanderthals >80 ka, in the genome of the Les Cottés Neanderthal.[16] Our results suggest the presence of multiple isolated late Neanderthal communities in Europe close to their time of extinction and shed light on their social organization, with limited, if any, level of interactions between different Neanderthal populations in their last millennia, even though these populations were geographically very close to each other.

RESULTS

Thorin is a late European Neanderthal

Grotte Mandrin is a rockshelter located in Mediterranean France directly overhanging the Rhône River Valley. The site records 12 main sedimentary layers dating from marine isotope stages (MISs) 5 to 3. Geological and micromorphological analyses show that all archeological levels were well preserved by rapid wind deposition of sands and silts.[1] The upper sequence is divided into eight archeological levels chronologically placed between 65.6 (base of layer F) and 41.5 ka cal. BP (calibrated years before present; layer B1), encompassing the last Neanderthal communities and the arrival of the first modern human groups. Each of these levels provide rich archeological records, totaling >60,000 lithics and 70,000 faunal remains. Fireplaces and hominin remains were also found in most of Grotte Mandrin's levels.[1] These eight archeological levels were divided into five cultural phases: level F: Rhodanian Quina, level E: Neronian, level D: Post-Neronian I (PNI), levels C2–B2: Post-Neronian II (PNII), and level B1: Protoaurignacian. The cultural determinations of the Neronian, PNI, and PNII phases at Grotte Mandrin[1] show major technical and cultural divergences with the coeval Mousterian and Châtelperronian societies[4] found in the neighboring regions of southwestern France and Burgundy.[3,5,18,19]

Thorin was discovered in 2015 at the entrance of the rockshelter in lateral contact between the upper layers and the bedrock in level B2 (Figure 1), associated with abundant fauna and artifacts attributed to the PNII, the last Mousterian phase from Grotte Mandrin.[1,3,5,18,19] Thorin is still under excavation but is already represented by several fragments, including a portion of the left palatal process at the level of the molars, a fragmentary mandible, and 31 permanent maxillary and mandibular teeth (Figure 2). While the upper right premolars and the upper right canine were lost postmortem, it is noteworthy that two supernumerary lower molars (fourth molars) are present. They are heteromorphic and exhibit a reduced and simplified (non-conical) crown with a single but large root from the cervix to the apex. The marked inclined wear facet affecting the occluso-mesial crown aspect of these two teeth fits with the distal interproximal facet of the lower third molars, indicating that the distomolars impacted the third molar crowns during the eruption process. Overall, the dental morphology of this individual is typical of Neanderthals, with shovel-shaped maxillary central incisors, marked labial convexity on the

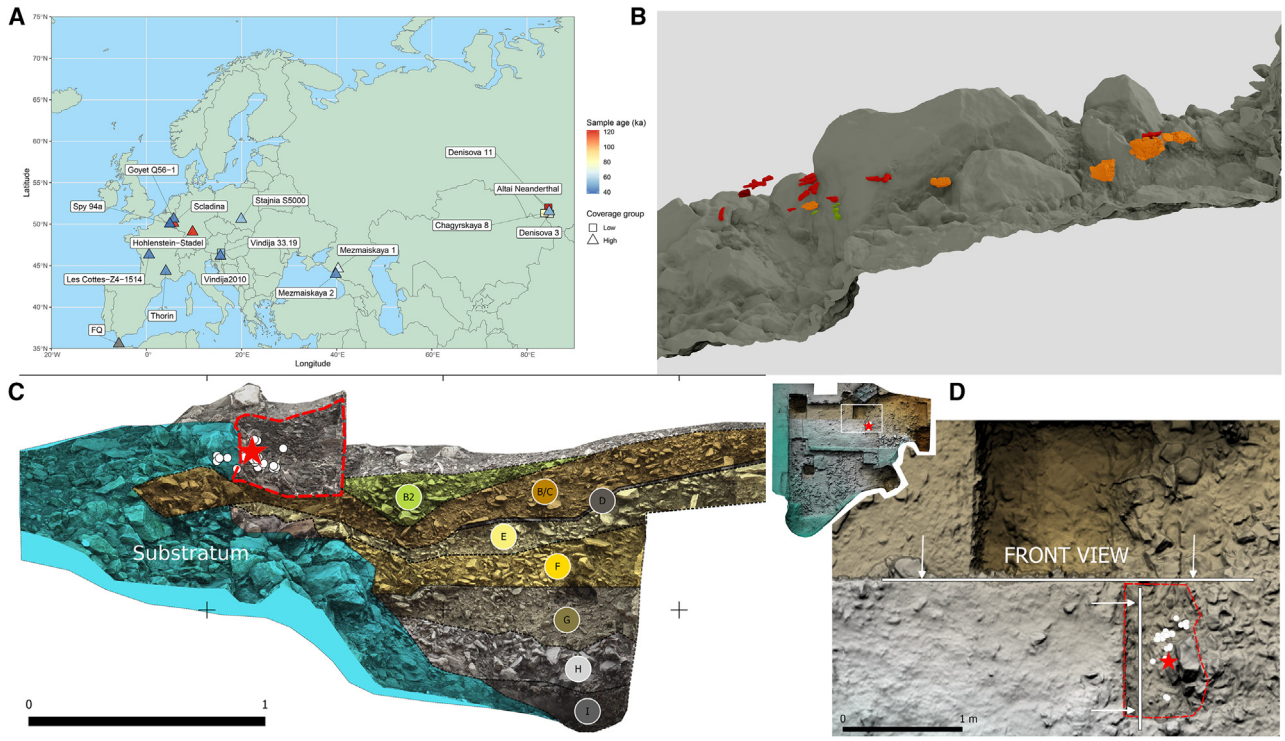

Figure 1. Map, plans, stratigraphy, and archeological 3D projections from Thorin in Grotte Mandrin

(A) Map showing geographic location, ages, and coverage group of Neanderthal fossils with genome-wide data used in this study.

(B) A 3D model of the disposition of the Thorin fossils during discovery.

(C and D) Stratigraphic (C) and plan (D) views through Grotte Mandrin showing Thorin's discovery location.

See also Figure S2 and supplemental information.

maxillary lateral incisors that also show a large tuberculum dentale on the lingual aspect of the crown, a well-developed hypocone projected lingually in the maxillary molars, and high root stem/branches ratio (i.e., taurodontism[20,21]; Figure S1). Most of the dentition shows advanced occlusal wear associated with hypercementosis at the root apex, notably on the anterior teeth, and the fully developed third and fourth molars indicate that it is an adult individual. The advanced occlusal wear is also associated with hypercementosis and exostoses on the maxilla, indicating that the teeth and jaw were under heavy (para)masticatory stress during the life of this individual. Near these cranial elements, the remains of five adult phalanges of the left hand were found (Figures 1 and S2). They showed typical Neanderthal features: ulnar deviation of the pollical distal phalanx and expansion of the distal phalangeal tuberosity.[22,23] All of the human remains recovered so far are of adult age, and the anatomical representation of the different elements is compatible with the presence of a single individual. While the teeth show typical Neanderthal features, the presence of two supernumerary fourth molars is remarkable. Mandibular distomolars are extremely rare in extant humans (around 0.02%),[24] and, to the best of our knowledge, have not been reported in Pleistocene *Homo* so far, although other kinds of supernumerary teeth have been described in a few instances for Neanderthal and Paleolithic modern humans.[25–28] The etiology of the presence of distomolars is still debated.[24] Studies of odontoskeletal anomalies found in early-generation hybrids of living primates display a relatively high incidence of distomolars.[29,30]

Recent analyses of Paleolithic sites in western Europe suggest that Mousterian lithic industries, traditionally attributed exclusively to Neanderthals, ended 39–41 ka cal. BP.[4] Throughout Eurasia, 10 sites have yielded Neanderthal remains directly dated between 50 and 40 ka cal. BP,[16,31–39] while only the four French sites—Arcy, Les Cottés, La Ferrassie, and Saint-Césaire—underwent ultrafiltration and provided ages between 45 and 40 ka cal. BP.[16,36,38,39] Neanderthal remains safely attributed to the final stage of their long existence are thus particularly rare and come essentially from sites excavated decades ago,[16,31–39] often with little or disputable stratigraphic and archeological context.

To provide a wider range of less-precious specimens for the destructive process of radiocarbon dating, we screened 30 fragmentary bone remains suspected as deriving from Thorin by zooarchaeology by mass spectrometry (ZooMS) collagen peptide mass fingerprinting[40,41] following the methods outlined by van der Sluis et al.[42] Specimens that yielded spectra matching a Hominidae signature[43] were radiocarbon dated at the Oxford Radiocarbon Accelerator Unit. Hydroxyproline was extracted for accelerator MS (AMS) dating to ensure reliability and contamination removal[44] (Table S1). A selection of hominin remains were also explored further by paleoproteomic sequencing and its ability to distinguish archaic from modern hominin taxa.[38] However,

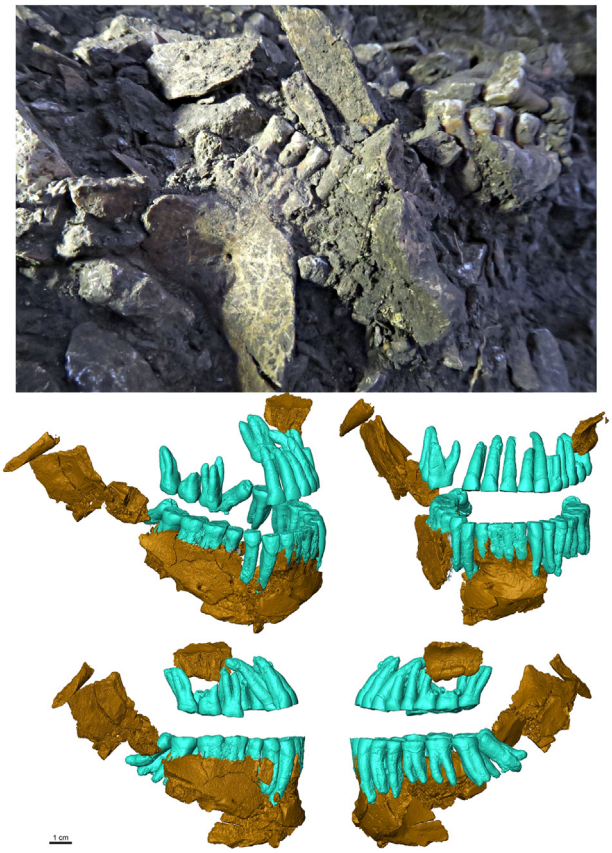

Figure 2. The Thorin Neanderthal

(Top) View of the mandible *in situ* when found in September 2019. (Bottom) Virtual reconstruction of the jaw and dental elements of Thorin in tilted (upper left), anterior (upper right), and lateral (bottom right and left) views.
See also Figure S2 and supplemental information.

comparisons with known modern human remains from Holocene deposits proved this approach to be problematic, having some direct implications on the *H. sapiens*/Neanderthal debate for the makers of the Châtelperronian culture, a technical tradition coeval with the PNII from Grotte Mandrin.

Direct uranium (U)-series dating and combined U-series-electron spin resonance (US-ESR) dating of Thorin was also undertaken on a fragment of the Neanderthal's lower left third premolar crown (Table S2). Additional faunal remains from level B2 were directly dated using the same approaches. U diffusion and accumulation patterns in the dentin and enamel were obtained prior to the isotopic analysis. According to the diffusion model and the U-series age distribution in the fossils, a minimum age of 43.5 ± 4.1 ka can be assigned to the Neanderthal remains from level B2. US-ESR modeling yields statistically indistinguishable finite ages of 48 + 5/−13 ka and 49 + 5/−10 ka for Thorin and the level B2 fauna, respectively (Table S3).

We undertook Bayesian modeling of the broader stratigraphic sequence at Grotte Mandrin to determine a robust age estimate for Thorin within the PNII levels (C2–B2). The model yielded an age range for Thorin of 51,300–48,900 cal. BP (at 68.2% probability) and 52,900–48,050 cal. BP (95.4% probability; Figure 3; see STAR Methods). It should be noted that the body is still under excavation. Its definitive attribution in a precise subphase in the PNII sequence (in between the different layers C and B) should be refined after its full excavation. If the model statistically places Thorin at ~52–48 ka, and then at the beginning of the PNII, the precise position of Thorin in the PNII may evolve further as the body appears in a small natural depression and could have been deliberately, or not, deposited here. At this stage, the most parsimonious and robust interpretation is certainly to consider Thorin as belonging to the PNII and therefore to a chronology positioned, in its maximum amplitude, between ~52 and 42 ka.

The carbon, nitrogen, oxygen, and strontium isotopic ratios measured on one of the Thorin teeth are fully compatible with an individual living in an open landscape and cold climatic conditions, consistent with the sedimentary characteristics of the C2–B2 deposits and direct dating results, rather than forested and temperate conditions, as would have been the case during MIS 5 (Figure S3; STAR Methods).

Thorin represents a distinct Neanderthal lineage

A first molar root fragment was used to generate a whole-genome sequence from Thorin by performing three sequential DNA extractions (E1, E2, and E3, Tables S4, and S5), drastically reducing modern human contamination (Tables S6, and S7), as well as whole-genome in-solution capture to increase the fraction of endogenous human DNA. Libraries built on raw (non-uracil-specific excision reagent [USER] treated) DNA extracts exhibited elevated terminal C>T/G>A substitution rates consistent with authentic ancient DNA data (STAR Methods; Figures S4–S9; Table S8). However, analyses of contamination rates using mtDNA and X chromosome data and grade-of-membership models on the nuclear DNA revealed substantial levels of modern human DNA contamination in the data generated from the first extract E1 (mtDNA-based estimate 13%–60%, Table S6; X-based estimate 13%–29%; Table S7). We therefore restricted all subsequent analyses to data from extracts E2 and E3, which show re-estimated mtDNA and nuclear contamination rates of <1% and 0.01%, respectively, yielding a final average depth of coverage of 1.3× of the nuclear genome and 561× for the mtDNA. We ruled out the potential of reference and capture bias in our data with D-statistics from which we in both cases obtain non-significant D-values (Figure S10; Table S9).

Molecular sex determination using reads mapped to the X and Y chromosomes showed that the Thorin individual was male (Table S10). Phylogenetic analyses of the mitochondrial genome revealed that the Thorin mitochondrial genome genome was most closely related to the recently described Stajnia S5000 individual from Poland[45] and the ~65 ka Mezmaiskaya 1 individual from the Caucasus,[8] distinct from other late western Eurasian Neanderthals[16] sequenced to date (Figure 4A). When including lower-coverage mitochondrial genomes using a phylogenetic maximum likelihood approach,[46] Thorin was most closely related to that of the Forbes' Quarry (FQ) individual from Gibraltar[47] in a clade with the Neanderthals from Galeria de las Estatuas (pit 1 layer 3 and pit 2 layer 2), Spain,[14] and the formerly mentioned Stajnia S5000 and Mezmaiskaya 1 (Figures S11 and S12), albeit with lower bootstrap support. Analysis of the Y

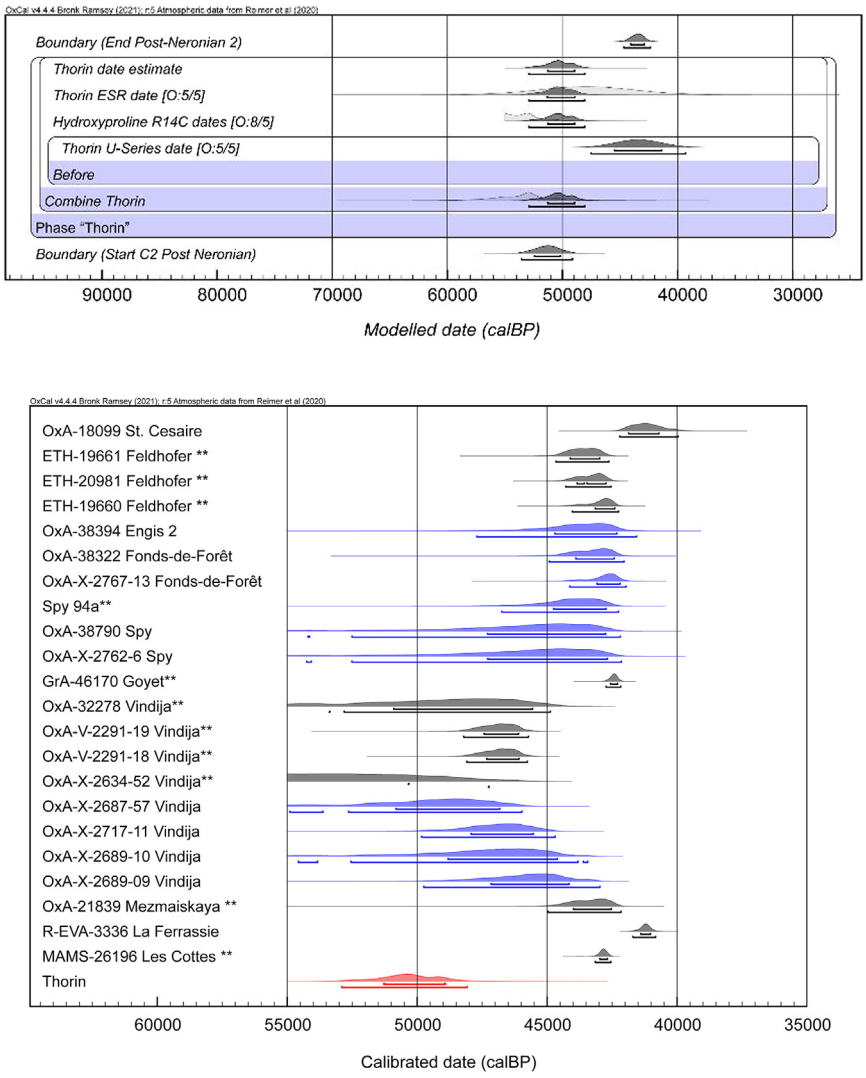

Figure 3. Bayesian modeling of Grotte Mandrin's PNII levels containing Thorin

(Top) The PNII phase of the Grotte Mandrin Bayesian model used to determine the age of Thorin. The direct ages on Thorin comprise 3 pooled mean hydroxyproline AMS ages, an ESR age, and a U-series age constrained as a minimum age (see Tables S1–S3). Outliers are included in the format [outlier:posterior/prior]. The boundaries are cross-referenced to the main Bayesian model established for the site, and represent the start and end dates of the PN2. (Bottom) Comparison of the Thorin modeled age against other late Neanderthals (see Table S12). Calibrated likelihoods in blue represent AMS dates obtained using HYP protocols. ** indicates high or low autosomal coverage of the dated specimen. Other likelihoods in black represent dates obtained on bulk or ultrafiltered/purified collagen samples. Dates are based on data from references 16 and 31–37. Related to Tables S1–S3 and S12.

chromosome showed a similar result, with the Thorin sequence diverging prior to the two male later Neanderthals, Spy94a and Mezmaiskaya 2[16] and forming a clade with the slightly earlier male Chagyrskaya Neanderthals[48] (Tables S11 and S12). We found that the Thorin Y chromosome sequence was most closely related to the El Sidrón 1253 Y chromosome sequence, in contrast to that individual's mitochondrial lineage placement among late European Neanderthals (Figures 4A and 4B). We caution, however, that this clade shows weaker support (89% bootstrap support), likely due to the low coverage for both samples. Using BEAST2,[49] we obtained a molecular age estimate of ~100 ka (Figures S13 and S14; Tables S13 and S14) for Thorin, some ~50 ka older than its archeostratigraphic context than the ^{14}C, U-series, and optically stimulated luminescence (OSL) ages obtained from the sediment layer from which Thorin was excavated. Similar discrepancies in ages have previously been observed for Chagyrskaya 8[15] and Stajnia S5000.[45] Notably, directly dated samples used for tip calibration are restricted to the clade of late Neanderthals (Figure 4A; Table S13) and cover only a shallow part of the entire tree, possibly leading to inaccurate estimates if substitution rates vary across the phylogeny.[50] To test this, we carried out an additional BEAST2 analysis including Thorin as an additional calibration point, using an age of 50 ka (95% confidence interval [CI]: 45–55 ka), allowing for variation in substitution rates along the tree. The resulting tip ages for Chagyrskaya 8 (70 ka; 95% CI: 48–94 ka) and Stajnia S5000 (77 ka; 95% CI: 53–103 ka) were found to be substantially closer to ages obtained from their respective archaeological contexts (~60 and ~50 ka). Similarly, the molecular age estimate of Mezmaiskaya 1 of ~74 ka also aligned with its previous estimate of 60–70 ka[51] (Figures S13 and S14; Tables S12 and S14). The estimated substitution rates remained within a relatively narrow range, suggesting that the initial molecular ages for samples in the Thorin mitochondrial clade were likely overestimated. Under this model, we estimate a divergence time of the Thorin clade of 123 ka (95% highest posterior density [HPD]: 97–152 ka), while we estimate the divergence between HST and the rest of the Neanderthals to 215 ka (95% HPD: 163–274 ka) and the split between modern humans and all Neanderthals to ~331 ka (95% HPD: 253–417 ka; Figures S13 and S14; Table S15).

We investigated broad population structure among the low-coverage Neanderthals and Chagyrskaya 8 by performing a Procrustes analysis on eigenvectors obtained from principal-component analysis,[52] where each individual was projected onto Vindija 33.19, Altai Neanderthal, and Denisova 3.[53] The projected individuals formed a cline toward Vindija 33.19, consistent with their previously reported sharing of a more recent common ancestor than with the Altai Neanderthal (Figure S15). Interestingly, the placement of Thorin fell within the cline but further

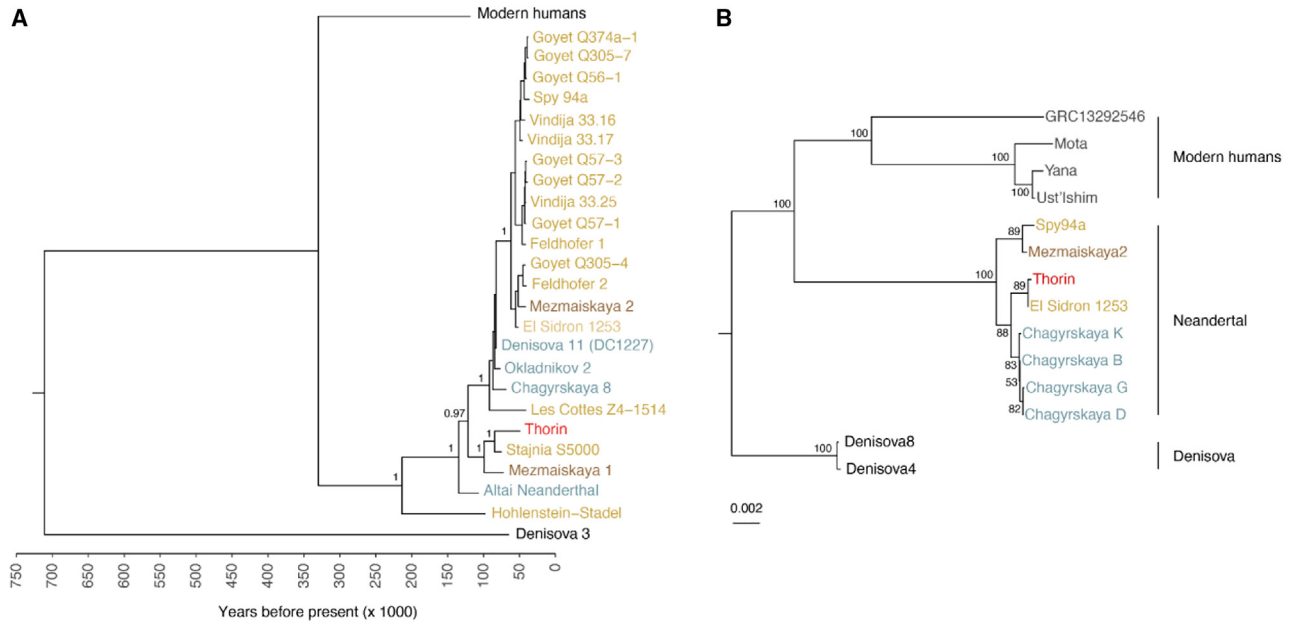

Figure 4. Mitochondrial and Y chromosome phylogenies of Thorin and published archaics

(A) A Bayesian phylogenetic tree of mitochondrial sequences restricted to the non-coding region from 24 Neanderthals, including Thorin, 1 Denisovan, and 73 modern humans. The tree is inferred from BEAST2, and the posterior probabilities are indicated for the deep divergences between the main Neanderthal clades. (B) Maximum likelihood tree of Y chromosome sequences based on 6,717 polymorphic SNPs from Thorin, 2 Denisovan, 8 Neanderthals including Thorin, and 4 modern humans, inferred using raxml-ng (Tables S11 and S14). Labels are colored based on region: yellow = Europe, green = Siberia, and brown = Caucasus. See also Figures S11 and S12 and Tables 11 and S14.

from Vindija 33.19 than any other late Neanderthal individual, suggesting a more distant relationship to Vindija 33.19. D-statistics using all reads confirmed that Neanderthals from Europe, the Caucasus, and Siberia younger than 80 ka shared significantly more genetic drift with Vindija 33.19 than with Thorin, indicating that Thorin belongs to a lineage that diverges earlier than the remaining late Neanderthals from the Vindija lineage. The finding was also supported when restricting to deaminated reads only (Figures 5 and S16–S21; Table S16). The exception was the low-coverage Neanderthal genome of FQ from Gibraltar,[47] which showed a weak but significant signal of excess allele sharing with Thorin, consistent with their closely related mitochondrial sequences (with the caveat of low coverage of the mitochondrial genome of FQ; Figures 5 and S11). Furthermore, Thorin does not show excess allele sharing with modern humans in comparison to all other west Eurasian Neanderthals, indicating that the lineage interbreeding with modern humans diverged prior to the Thorin lineage, and ruling out the possibility of recent interbreeding with early modern humans at Grotte Mandrin Cave[1] (Figures S10 and S17).

We carried out demographic modeling using the site frequency spectrum-based approach implemented in momi2,[54] which allows the placement of low-coverage individuals onto a scaffold inferred from high-quality genomes. We first fit a scaffold demography including the three high-coverage Neanderthals (Altai Neanderthal, Chagyrskaya 8, and Vindija 33.19) as well as the Denisovan, incorporating previously inferred demographic events.[8] The low-coverage samples Thorin and Mezmaiskaya 1 were then added to this scaffold, allowing for a divergence from the Vindija 33.19 lineage at any point after the split from the Altai Neanderthal. The best-fit model indicates a divergence of the Thorin lineage from Vindija 33.19 at 102,861 years ago (95% CI: 100,267–105,169), considerably earlier than those of Mezmaiskaya 1 (82,617 years ago; 95% CI: 79,313–85,606) or Chagyrskaya 8 (79,458 years ago; 95% CI: 77,600–80,892), and consistent with results from D-statistics and mtDNA (Figure 6; Tables S17 and S18). When adding the FQ Neanderthal to the demography, we find that a model for it diverging from the Thorin lineage (~81 ka) is better supported than one where it diverges independently from the ancestral lineage (~106 ka; log likelihood difference = 11; Figure S22), consistent with the D-statistic results.

Using a novel approach to detect runs of homozygosity in low-coverage Neanderthal genomes, we found evidence for increased homozygosity in the Thorin genome compared to other late European Neanderthals. Thorin harbors ~7% of its genome in homozygous segments of ≥5 Mb, including 45 Mb (~1.5%) in segments longer than 20 Mb, indicative of recent inbreeding (Figures 7 and S23–S25). Taken together, our results suggest small group sizes and long-term genetic isolation of the Thorin population from other late Neanderthal populations with genomic data available.

Other isolated lineages present 50 ka?

We further investigated the possibility of population turnover in Europe during the late Neanderthal period. Using D-statistics

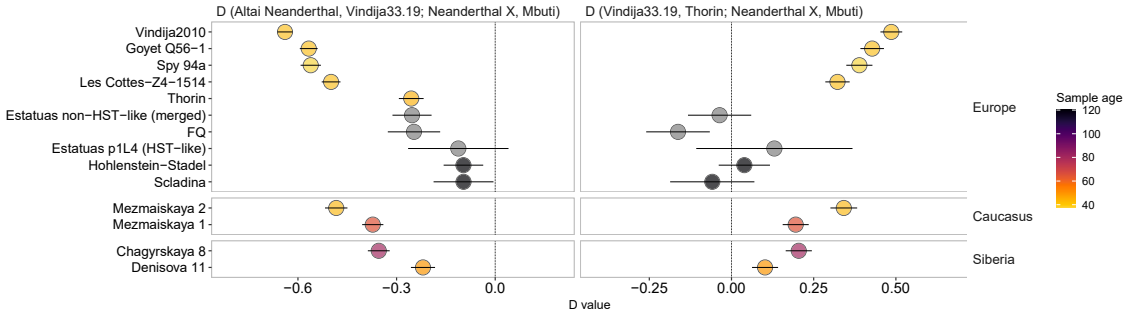

Figure 5. Allele sharing between Thorin and other known Neanderthals

(Left) D-statistics of the form D (Altai Neanderthal, Vindija 33.19; Neanderthal X, Mbuti), showing that all Eurasian Neanderthal samples share more alleles with Vindija 33.19 than with the Altai Neanderthal. Thorin shares relatively more alleles with Vindija 33.19 than early European Neanderthals of the putative first radiation (HST, Scladina, Estatuas pit 1 layer 4), but less than the second radiation (Mezmaiskaya 1, Chagyrskaya 8). We used all reads obtained from each Neanderthal X case to maximize the resolution as contamination levels in general are low. Chagyrskaya 8 is, however, represented with diploid genotypes. (Right) D-statistics of the form D (Vindija 33.19, Thorin; Neanderthal X, Mbuti), showing that Neanderthals from Europe, the Caucasus, and Siberia younger than 80 ka share more alleles with Vindija 33.19 than with Thorin. The exception is the Gibraltar Neanderthal sample (FQ), which shows increased affinity with Thorin. We used all reads for each Neanderthal X and Thorin, while we represented Vindija 33.19 with pseudo-haploid genotypes. Error bars indicate 3× SE ($|Z| = 3$). Colors indicate the age of the individuals. Samples not directly dated or with uncertain dates are indicated with gray circles.

See also Figures S10 and S16–S20 and Table S12.

testing whether the late Caucasus lineage of Mezmaiskaya 2 formed an outgroup to other late European Neanderthals, we found evidence of gene flow with a Neanderthal lineage, diverging prior to the most recent common ancestor of the late Neanderthals, in the ~43 ka Les Cottés Z4-1514 sample from France (Figure S20). Interestingly, this individual carries an mtDNA lineage most closely related to the Siberian Neanderthals from Okladnikov and Chagyrskaya Caves, diverging earlier than the clade of Vindija-like late Neanderthals sampled to date (Figure 4). Demographic modeling of Les Cottés Z4-1514 and Mezmaiskaya 2 onto the previous best-fitting model revealed that a model with gene flow into Les Cottés Z4-1514 from a previously unsampled lineage diverging at ~89 ka provided a significantly better fit than one without gene flow (log likelihood difference = 72; Figure S26). An alternative model involving a previously unsampled lineage constrained to diverging from the Thorin lineage also yielded a poorer fit, with a divergence time of the previously unsampled lineage close to the diverging of the Thorin lineage (log likelihood difference = 11; Figure S26). Our results thus suggest the presence of at least two lineages with divergence dates of at least 89 ka, which stayed genetically isolated in close geographic proximity during the late Neanderthal period, and subsequently were partially replaced by an expansion of Vindija-like lineages into western Europe within the last 10 ka of their existence. Interestingly, the eastern European late Neanderthal from Mezmaiskaya Cave (Mezmaiskaya 2) also shows high levels of homozygosity (Figure 7), suggesting that small group sizes were likely also common among late Neanderthals outside the expanding Vindija-like population.

DISCUSSION

Thorin is the most complete Neanderthal individual found in France since 1979[17] and falls among a group of other Neanderthals dating to the last millennia of their existence in western Europe. So far, population genetic analysis of other late Neanderthals has indicated that they belonged to a single metapopulation with no significant evidence of population structure among them.[16] The genome of Thorin sheds new light on the population structure of late Neanderthals, as our genomic analyses demonstrate that Thorin belongs to a lineage diverging ~100–105 ka from the ancestral European Neanderthal lineage, and thereby represents a remnant of earlier European Neanderthals. Interestingly, the timing of divergence of this lineage coincides with the MIS 5 interglacial, a period in which fast climatic and environmental changes across Eurasia and repopulation by warm adapted fauna occurred throughout the continent.[55,56] The timing of this divergence also coincided with a period of population replacement detected in northern Spain among Neanderthal populations.[14]

Our analysis testing for gene flow between Thorin's lineage and other known Neanderthal and modern human lineages suggests the existence of an isolated group of late Neanderthals in western Europe 50 ka. This population is associated with a distinctive PNII lithic tradition,[1] which is continuously attested to in the last four Mousterian levels of Grotte Mandrin (levels C2–B2), from 52.9 to 43.0 ka at 95% CI, overlapping with the final disappearance of Neanderthal populations in Eurasia.[1,4] Thorin, therefore, likely belonged to one of the last representative Neanderthal populations in this area of Mediterranean France, and is the first direct genomic evidence of population structure among late European Neanderthals. The genetic relationship observed between Thorin and the low-coverage genome of FQ (also indicated in demographic modeling) suggests that the Gibraltar Neanderthals might have been members of an extended southwest European metapopulation, and raises the possibility of a much later dating for those individuals than previously anticipated.[47] The 50-ka-long genetic isolation of the Thorin lineage raises new questions of relevance to the Neanderthal extinction debate and the types of interactions among Neanderthal populations and also with the earliest *H. sapiens* arriving in Europe. It remains unknown whether this population was only locally spread in the middle Rhône Valley or whether the Thorin lineage was more

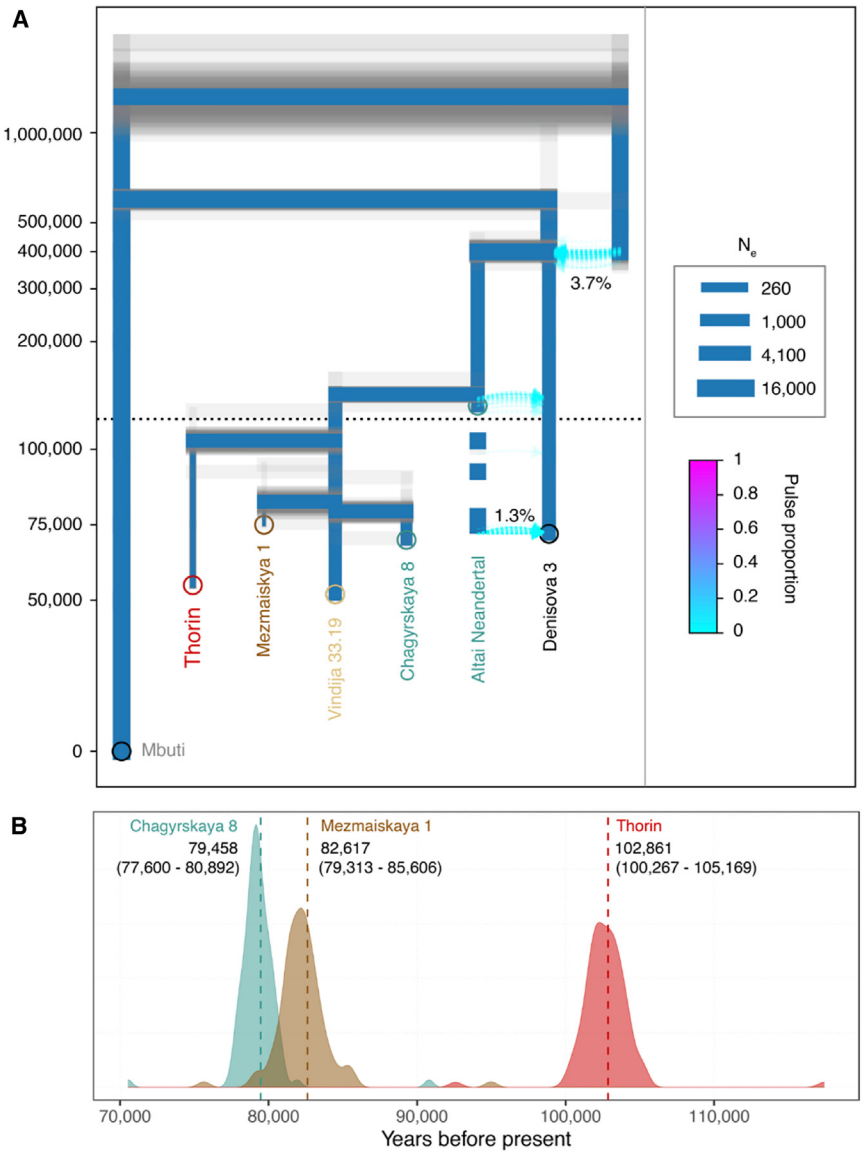

Figure 6. Demographic history of the Thorin lineage

(A) Best-fitting demographic model inferred using momi2 relating Thorin to other Neanderthal and Denisovan genomes. Blue branches show point estimates, whereas gray transparent branches indicate estimates obtained using 100 nonparametric bootstrap replicates. Results are based on a set of 2,454,271 transversion SNPs, with the lower-coverage samples Thorin and Mezmaiskaya 1 represented by pseudo-haploid genotypes.

(B) Point estimates (dashed line) and density of 100 parametric bootstrap replicates for divergence time parameters of Thorin, Mezmaiskaya 1, and Chagyrskaya 8 Neanderthal genomes from the late European Neanderthal Vindija 33.19.

See also Figures S13, S14, S22, and S26 and Tables 15 and S17.

widely distributed across Europe, as suggested by the Gibraltar connections. It is noteworthy that the PNII has no clear technical local roots in older traditions from the Rhône Valley—the PNI (layer D), the Neronian (layer E), and the Rhodanian Quina (layer F)—showing strong technical and cultural divergences with the PNII. This may indicate an exotic origin of these PNII traditions. Direct comparisons between the PNII and the lithic data from Gibraltar could highlight whether these genetic connections are also related to cultural connections between these late Neanderthal populations in the western Mediterranean region.

The sedimentary autosomal DNA data from the Galeria de las Estatuas population was unfortunately not of sufficient coverage to establish closer affinity with Thorin. However, the sampling locations of European Neanderthals within the mtDNA clade of Thorin, from Iberia (Gibraltar, Galeria de las Estatuas) and southern France to Poland (Stajnia), would support a broader distribution and be consistent with a suggested radiation of Neanderthal populations at ~105 ka, although we note that the mitochondrial genomes of FQ and Estatuas are of low coverage and thus should be treated with caution. While it is commonly inferred that the interactions between the first *H. sapiens* and the last Neanderthals may have played an important role in the latter's extinction in Europe, the identification of a hitherto unrecognized late Neanderthal population and the demonstration of the genetic and cultural isolation of these Neanderthal groups reveal an unexpected population structure among late Neanderthals and raises new lines of questions to explore further their social and ethological organization, which could have played an important role in their later extinction.

Besides the lineage that is represented by Thorin, our demographic modeling provides indirect evidence of the presence of another previously unsampled diverged European lineage through introgression in the French Neanderthal Les Cottés. Our demographic modeling suggests that this introgressing lineage diverged some time after the Thorin lineage, closer to the divergence of Mezmaiskaya1 and the Siberian individual Chagyrskaya 8 from the Altai region, with which Les Cottés also shares a closely related mitochondrial lineage. Whether this previously unsampled lineage forms part of an as yet unknown further radiation of lineages after 100 ka but before the classical late Neanderthals remains unknown without a denser sampling of genomic data from around that time period. Our results nevertheless suggest a minimum of two, but possibly three, distinct Neanderthal lineages present in Europe during the late Neanderthal period. In the absence of any detectable gene flow between Thorin and other Neanderthal lineages after its divergence, we conclude that Thorin represents a lineage that possibly stayed isolated for ~50 ka.

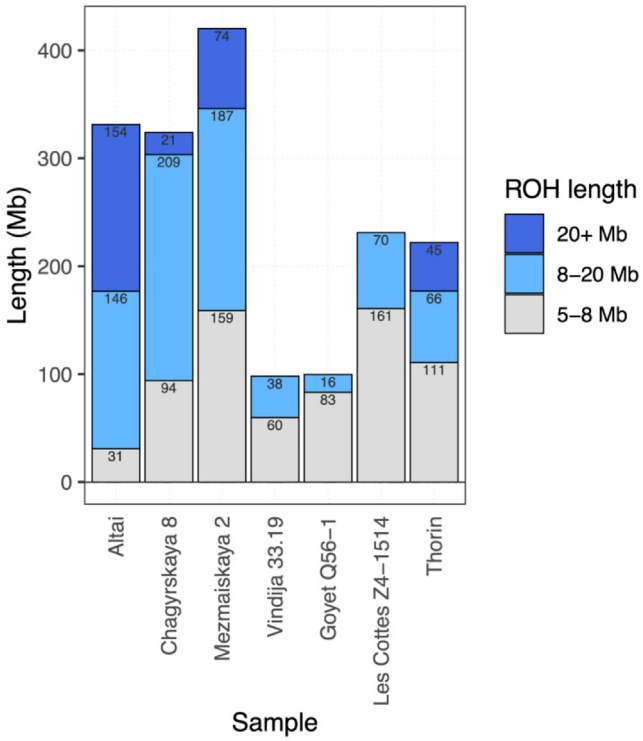

Figure 7. Runs of homozygosity (ROH) in Neanderthals

Bar plot showing cumulative total length of ROHs ≥5 Mb in Thorin and other Neanderthal genomes with average genomic coverage ≥1.5×. ROH length classes are distinguished by bar colors, with total length in each class indicated.

See also Figures S23–S25.

Socially speaking, the absence of recent *H. sapiens* introgression within late Neanderthal populations could have been part of a larger pattern affecting the latter, which seem to have limited or avoided gene exchange not only with early *H. sapiens* but, more generally, within Neanderthal populations themselves. Anthropologically, these gene exchange processes are never limited to a love affair between two individuals, but systematically correspond to the alliances that human populations consciously decide to build.[57] The absence of gene exchanges, or their non-reciprocity (presence of Neanderthal genes in the first *H. sapiens* in Europe, with no reciprocity in the last Neanderthals), raises questions about the social structures that governed these Neanderthal populations. Our results thus suggest that small isolated populations with, and potentially without, limited inter-group exchanges, may well represent a surprising and more general feature of Neanderthal social structures.

Culturally speaking, deep technical specificities distinguishing Rhône Valley late Mousterian industries have long been proposed,[18,19,58] emphasizing that from MIS 5 to 3 these French Mediterranean Neanderthal societies possessed a distinct cultural background. These cultural traits distinguishing Neanderthal societies from neighboring regions can now be paralleled with long-term genetic isolation between these societies. These genetic differences may signify a major process of population replacement following or related to the expansion of anatomically modern humans through Europe. Interestingly, Thorin corresponds to the phases of Neanderthal reoccupation of Grotte Mandrin after the earliest modern human incursions in the continent.[1,2] This genetic but also cultural evidence suggests the possibility of the presence of multiple genetically isolated Neanderthal lineages over millennia. The PNII cultural traditions of the Thorin population overlap with the Châtelperronian chronology dating to ~45–40 ka[1,4,5] absent from the Rhône Valley but recognized in a large region stretching from Burgundy to the Mediterranean and Atlantic Spain and that was classically attributed to late Neanderthal traditions.[1,4,5] In 2023, it was proposed that the Châtelperronian was not of Neanderthal origin but was closely linked with northern Early Ahmarian industries from Lebanon, an eastern Mediterranean tradition closely associated with modern humans.[5] The Châtelperronian would then signal a second wave of *H. sapiens* migration in the continent and should not be associated with Neanderthal populations. This three-wave model has since been supported by the discovery of a *H. sapiens* ilium bone in a Châtelperronian layer from Burgundy, north of Grotte Mandrin. These data draw a striking picture of late Neanderthals and their coeval *H. sapiens* populations, where small populations of Neanderthals appear to have been isolated during tens of millenia, both culturally and genetically, leading to an increase in homozygosity levels. The intergroup network of these late Neanderthals appears much more constrained than the large social interconnections visible among *H. sapiens* populations, where trans-Mediterranean cultural correspondences can be drawn during the three earliest phases of their colonization of Europe from ~55 to 40 ka.[5] These genetic, social, and cultural divergences among these populations may have induced fragilities among long-isolated Neanderthal groups facing sapiens populations structurally organized on large and complex social networks.[1] Much more than an event, the decline of the Neanderthals would then represent a complex process where the history and ethology of these populations may have played a key role in the structure of their remarkable extinctions.

Limitations of the study

This study has presented a low-coverage genome of a late Neanderthal discovered in Grotte Mandrin, Mediterranean France, whose nuclear genome has allowed the identification of a long-term isolated genetic lineage in western Europe. We estimated the age of Thorin by combining several dating methods and the construction of a Bayesian model for the stratigraphic context in which the remains are found. However, these dating methods have some large SDs. Moreover, the remains are still under excavation, and the body appears in a small natural depression where he could have been deliberately, or not, deposited, impacting the stratigraphic age evaluation of the remains. A parsimonious approach is, at this stage, to consider its precise chronology as statistically constrained somewhere between 52 and 42 ka. The age of Thorin should then be refined in the future according to its definitive attribution to layer B or C. If attributed to layer B, then the body would then have been deposited in a little natural depression. If attributed to layer C, then this natural depression would represent a very localized natural

deformation of the layer occuring after the death of Thorin. Layers B and C both belong to the PNII culture. The attribution of Thorin to layer B or C then has no impact on its cultural attribution to the PNII and its attribution to the very last phase of the Mousterian in that region. The most recent field campaign (summer 2023) allowed the recovery of some additional Thorin remains stratigraphically well constrained in the very upper part of layer B (layer B2). These recent findings strongly suggest that Thorin is more likely to be ~42 ka old rather than ~50 ka old, and would then represent one of the very last Neanderthals in this region.

In this study, we draw the conclusion that the population structure among late Neanderthals was more complex than previously thought. While a single genome is sufficient to establish the presence of a novel, distinct genetic lineage among late Neanderthal individuals, it only offers a single observation of the larger population it belonged to and might not be fully representative of its full genetic diversity. This is a more general concern with studies on archaic hominins, as remains from which DNA has been successfully recovered remain sparse. Nonetheless, we point to the finding of the FQ Neanderthal whose low-coverage mitochondrial genome likewise suggests the presence of a distinct lineage in western Europe. We furthermore argue that the lineage of Thorin has been genetically isolated based on elevated homozygosity across his genome. The approach we used performed well using simulated low-coverage genomes, but we caution that the inferred distributions of homozygous segment lengths could still be affected by the low coverage. In the future, denser sampling and deeper sequencing of Neanderthals will be needed to gain a deeper understanding of the genomic history of the Neanderthals.

STAR★METHODS

Detailed methods are provided in the online version of this paper and include the following:

- KEY RESOURCES TABLE
- RESOURCE AVAILABILITY
  - Lead contact
  - Materials availability
  - Data and code availability
- EXPERIMENTAL MODEL AND STUDY PARTICIPANT DETAILS
  - Ancient samples
- METHOD DETAILS
  - X-Ray microtomographic scanning of the teeth
  - ZooMS collagen fingerprinting
  - Paleoproteomic analyses
  - Sample dating
  - Isotopic analyses (C, O, Sr)
  - Sample processing for DNA sequencing
  - DNA sequencing data analysis
  - Sequencing data authentication and contamination estimation
  - Mitochondrial DNA (mtDNA) and Y chromosome analysis
  - mtDNA analysis
  - Population genetic analyses

SUPPLEMENTAL INFORMATION

Supplemental information can be found online at https://doi.org/10.1016/j.xgen.2024.100593.

ACKNOWLEDGMENTS

We deeply acknowledge the Service Régional de l'Archéologie Auvergne Rhône-Alpes, the city of Malataverne, and all of the students/volunteers who supported the 30 years of continuous field research in Grotte Mandrin. The authors acknowledge Professors Eske Willerslev and Ludovic Orlando for fruitful discussions and continuous support. We thank the laboratory technicians of the Danish National High-throughput DNA Sequencing Center, as well as Tina B. Brand, Pernille V.S. Olsen, and Jesper Stenderup from the Lundbeck Foundation Center for GeoGenetics for technical assistance. Thanks also go to Manasij Pal Chowdhury and members of the University of Manchester Biological Mass Spectrometry core facility for assisting with proteomic file management. Long-term research was supported by the Service Régional de l'Archéologie Auvergne Rhône-Alpes, the French CNRS, and the city of Malataverne. The 3D site models were granted by the city of Malataverne and the Auvergne Rhône-Alpes region. Genetic analyses were supported by the Lundbeck Foundation and the Danish National Research Foundation (DNRF94). A.S.-O. is supported by the European Research Council (ERC; StG2023-101117101 anthropYXX). The geochronology research was supported by the ERC under the Seventh Framework Program (FP7/2007-2013) grant no. 324139 ("PalaeoChron") awarded to T.H. and the Australian Research Council Future Fellowship grant FT200100816 to M.D. and L.J.A.

AUTHOR CONTRIBUTIONS

L.S. and L.M. led the scientific project and excavated the site. Microtomographic-based data were collected and analyzed by C.Z. L.S. analyzed the lithic technical systems. H. Coqueugniot, O.D., and C.Z. studied the human remains. Spatial analyses were performed by P.Y. and X.M. H. Camus recorded and analyzed the stratigraphy and deposit dynamics. Radiometric dating analyses and Bayesian age modeling were performed by T.H., R.J.-B., L.J.A., M.D., M.F., T.D., and D.C. H.B. performed and interpreted the isotopic measurements on bones and teeth. M.S. coordinated the ancient DNA analyses. A.S.-O. performed the ancient DNA laboratory work and sequencing. T.V. and M.S. analyzed the genomic data. L.S., C.Z., M.S., T.V., and J.E.L. wrote the manuscript, with contributions from all other authors. A.S.-O., T.V., and L.S. wrote the supplementary materials, with contributions from all other authors.

DECLARATION OF INTERESTS

The authors declare no competing interests.

Received: April 4, 2023
Revised: November 23, 2023
Accepted: June 5, 2024
Published: September 11, 2024

REFERENCES

1. Slimak, L., Zanolli, C., Higham, T., Frouin, M., Schwenninger, J.L., Arnold, L.J., Demuro, M., Douka, K., Mercier, N., Guérin, G., et al. (2022). Modern human incursion into Neanderthal territories 54,000 years ago at Mandrin, France. Sci. Adv. *8*, eabj9496. https://doi.org/10.1126/sciadv.abj9496.
2. Metz, L., Lewis, J.E., and Slimak, L. (2023). Bow-and-arrow, technology of the first modern humans in Europe 54,000 years ago at Mandrin, France. Sci. Adv. *9*, eadd4675. https://doi.org/10.1126/sciadv.add4675.
3. Slimak, L. (2019). For a cultural anthropology of the last Neanderthals. Quat. Sci. Rev. *217*, 330–339. https://doi.org/10.1016/j.quascirev.2018.12.019.
4. Higham, T., Douka, K., Wood, R., Ramsey, C.B., Brock, F., Basell, L., Camps, M., Arrizabalaga, A., Baena, J., Barroso-Ruíz, C., et al. (2014). The timing and spatiotemporal patterning of Neanderthal disappearance. Nature *512*, 306–309. https://doi.org/10.1038/nature13621.

5. Slimak, L. (2023). The three waves: Rethinking the structure of the first Upper Paleolithic in Western Eurasia. PLoS One *18*, e0277444. https://doi.org/10.1371/journal.pone.0277444.

6. Slimak, L. (2008). The Neronian and the historical structure of cultural shifts from Middle to Upper Palaeolithic in Mediterranean France. J. Archaeol. Sci. *35*, 2204–2214. https://doi.org/10.1016/j.jas.2008.02.005.

7. Ríos, L., Kivell, T.L., Lalueza-Fox, C., Estalrrich, A., García-Tabernero, A., Huguet, R., Quintino, Y., de la Rasilla, M., and Rosas, A. (2019). Skeletal Anomalies in The Neandertal Family of El Sidrón (Spain) Support A Role of Inbreeding in Neandertal Extinction. Sci. Rep. *9*, 1697. https://doi.org/10.1038/s41598-019-38571-1.

8. Prüfer, K., Racimo, F., Patterson, N., Jay, F., Sankararaman, S., Sawyer, S., Heinze, A., Renaud, G., Sudmant, P.H., De Filippo, C., et al. (2014). The complete genome sequence of a Neanderthal from the Altai Mountains. Nature *505*, 43–49. https://doi.org/10.1038/nature12886.

9. Sikora, M., Seguin-Orlando, A., Sousa, V.C., Albrechtsen, A., Korneliussen, T., Ko, A., Rasmussen, S., Dupanloup, I., Nigst, P.R., Bosch, M.D., et al. (2017). Ancient genomes show social and reproductive behavior of early Upper Paleolithic foragers. Science *358*, 659–662. https://doi.org/10.1126/science.aao1807.

10. Ringbauer, H., Novembre, J., and Steinrücken, M. (2021). Parental relatedness through time revealed by runs of homozygosity in ancient DNA. Nat. Commun. *12*, 5425. https://doi.org/10.1038/s41467-021-25289-w.

11. Green, R.E., Krause, J., Briggs, A.W., Maricic, T., Stenzel, U., Kircher, M., Patterson, N., Li, H., Zhai, W., Fritz, M.H.Y., et al. (2010). A draft sequence of the neandertal genome. Science *328*, 710–722. https://doi.org/10.1126/science.1188021.

12. Prüfer, K., De Filippo, C., Grote, S., Mafessoni, F., Korlević, P., Hajdinjak, M., Vernot, B., Skov, L., Hsieh, P., Peyrégne, S., et al. (2017). A high-coverage Neandertal genome from Vindija Cave in Croatia. Science *1887*, 1–13. https://doi.org/10.1126/science.aao1887.

13. Peyrégne, S., Slon, V., Mafessoni, F., De Filippo, C., Hajdinjak, M., Nagel, S., Nickel, B., Essel, E., Le Cabec, A., Wehrberger, K., et al. (2019). Nuclear DNA from two early Neandertals reveals 80,000 years of genetic continuity in Europe. Sci. Adv. *5*. https://doi.org/10.1126/sciadv.aaw5873.

14. Vernot, B., Zavala, E.I., Gómez-Olivencia, A., Jacobs, Z., Slon, V., Mafessoni, F., Romagné, F., Pearson, A., Petr, M., Sala, N., et al. (2021). Unearthing Neanderthal population history using nuclear and mitochondrial DNA from cave sediments. Science *372*, eabf1667. https://doi.org/10.1126/science.abf1667.

15. Mafessoni, F., Grote, S., de Filippo, C., Slon, V., Kolobova, K.A., Viola, B., Markin, S.V., Chintalapati, M., Peyrégne, S., Skov, L., et al. (2020). A high-coverage Neandertal genome from Chagyrskaya Cave. Proc. Natl. Acad. Sci. USA *117*, 15132–15136. https://doi.org/10.1073/pnas.2004944117.

16. Hajdinjak, M., Fu, Q., Hübner, A., Petr, M., Mafessoni, F., Grote, S., Skoglund, P., Narasimham, V., Rougier, H., Crevecoeur, I., et al. (2018). Reconstructing the genetic history of late Neanderthals. Nature *555*, 652–656. https://doi.org/10.1038/nature26151.

17. Léve^que, F., and Vandermeersch, B. (1980). Les découvertes de restes humains dans un horizon castelperronien de Saint-Césaire (Charente-Maritime). Bull. Soc. Prehist. Fr. *77*, 187–189.

18. Slimak, L. (1999). Pour une individualisation des Moustériens de type Quina dans le quart sud-est de la France? La Baume Néron (Soyons, Ardeche) et le Champ Grand (Saint-Maurice-sur-Loire, Loire), premieres données. bspf. *96*, 133–144.

19. Slimak, L. (2004). Les Dernieres Expressions du Moustérien entre Loire et Rho^ne. Phd thesis (Université de Provence).

20. Bailey, S.E. (2002). A closer look at Neanderthal postcanine dental morphology: The mandibular dentition. Anat. Rec. *269*, 148–156. https://doi.org/10.1002/ar.10116.

21. Bailey, S.E. (2004). Derived morphology in Neanderthal maxillary molars: Insights from above. Am. J. Phys. Anthropol. *123*, 57.

22. Musgrave, J.H. (1973). The phalanges of Neanderthal and Upper Palaeolithic hands, H. Evolution and M.H. Day, eds. (Taylor and Francis), pp. 59–85.

23. Trinkaus, E. (1982). The Shanidar 3 Neandertal. Am. J. Phys. Anthropol. *57*, 37–60.

24. Vázquez Mosquerira, V.M., Espinosa Meléndez, M.T., and Hernández Flores, F. (2018). Presence of the fourth molar. Literature review. Rev. Odont. Mex. *22*, 103–117.

25. Legoux, P. (1974). Étude odontologique des restes humains périgordiens et proto-magdaléniens de l'Abri-Pataud (Dordogne) (seconde partie). bmsap. *1*, 45–84.

26. Smith, T.M., Reid, D.J., Olejniczak, A.J., Bailey, S., Glantz, M., Viola, B., and Hublin, J.J. (2011). Dental Development and Age at Death of a Middle Paleolithic Juvenile Hominin from Obi-Rakhmat Grotto, Uzbekistan. In Continuity and Discontinuity in the Peopling of Europe, S. Condemi and G.C. Weniger, eds. (Springer), pp. 155–163.

27. Trinkaus, E. (2018). An abundance of developmental anomalies and abnormalities in Pleistocene people. Proc. Natl. Acad. Sci. USA *115*, 11941–11946. https://doi.org/10.1073/pnas.1814989115.

28. Trinkaus, E., Formicola, V., Svoboda, J., Hillson, S.W., and Holliday, T.W. (2001). Dolnı Věstonice 15: Pathology and Persistence in the Pavlovian. J. Archaeol. Sci. *28*, 1291–1308. https://doi.org/10.1006/jasc.2001.0678.

29. Ackermann, R.R., Schroeder, L., Rogers, J., and Cheverud, J.M. (2014). Further evidence for phenotypic signatures of hybridization in descendant baboon populations. J. Hum. Evol. *76*, 54–62. https://doi.org/10.1016/j.jhevol.2014.05.004.

30. Ackermann, R.R., Arnold, M.L., Baiz, M.D., Cahill, J.A., Cortés-Ortiz, L., Evans, B.J., Grant, B.R., Grant, P.R., Hallgrimsson, B., Humphreys, R.A., et al. (2019). Hybridization in human evolution: Insights from other organisms. Evol. Anthropol. *28*, 189–209. https://doi.org/10.1002/evan.21787.

31. Schmitz, R.W., Serre, D., Bonani, G., Feine, S., Hillgruber, F., Krainitzki, H., Pääbo, S., and Smith, F.H. (2002). The Neandertal type site revisited: interdisciplinary investigations of skeletal remains from the Neander Valley, Germany. Proc. Natl. Acad. Sci. USA *99*, 13342–13347. https://doi.org/10.1073/pnas.192464099.

32. Pinhasi, R., Higham, T.F.G., Golovanova, L.V., and Doronichev, V.B. (2011). Revised age of late Neanderthal occupation and the end of the Middle Paleolithic in the northern Caucasus. Proc. Natl. Acad. Sci. USA *108*, 8611–8616. https://doi.org/10.1073/pnas.1018938108.

33. Rougier, H., Crevecoeur, I., Beauval, C., Posth, C., Flas, D., Wißing, C., Furtwängler, A., Germonpré, M., Gómez-Olivencia, A., Semal, P., et al. (2016). Neandertal cannibalism and Neandertal bones used as tools in Northern Europe. Sci. Rep. *6*, 29005. https://doi.org/10.1038/srep29005.

34. Deviese, T., Karavanić, I., Comeskey, D., Kubiak, C., Korlević, P., Hajdinjak, M., Radović, S., Procopio, N., Buckley, M., Pääbo, S., and Higham, T. (2017). Direct dating of Neanderthal remains from the site of Vindija Cave and implications for the Middle to Upper Paleolithic transition. Proc. Natl. Acad. Sci. USA *114*, 10606–10611. https://doi.org/10.1073/pnas.1709235114.

35. Jaouen, K., Richards, M.P., Le Cabec, A., Welker, F., Rendu, W., Hublin, J.J., Soressi, M., and Talamo, S. (2019). Exceptionally high δ^{15}N values in collagen single amino acids confirm Neanderthals as high-trophic level carnivores. Proc. Natl. Acad. Sci. USA *116*, 4928–4933. https://doi.org/10.1073/pnas.1814087116.

36. Balzeau, A., Turq, A., Talamo, S., Daujeard, C., Guérin, G., Welker, F., Crevecoeur, I., Fewlass, H., Hublin, J.J., Lahaye, C., et al. (2020). Pluridisciplinary evidence for burial for the La Ferrassie 8 Neandertal child. Sci. Rep. *10*, 21230. https://doi.org/10.1038/s41598-020-77611-z.

37. Deviese, T., Abrams, G., Hajdinjak, M., Pirson, S., De Groote, I., Di Modica, K., Toussaint, M., Fischer, V., Comeskey, D., Spindler, L., et al.

(2021). Reevaluating the timing of Neanderthal disappearance in Northwest Europe. Proc. Natl. Acad. Sci. USA *118*, e2022466118. https://doi.org/10.1073/pnas.2022466118.

38. Welker, F., Hajdinjak, M., Talamo, S., Jaouen, K., Dannemann, M., David, F., Julien, M., Meyer, M., Kelso, J., Barnes, I., et al. (2016). Palaeoproteomic evidence identifies archaic hominins associated with the Châtelperronian at the Grotte du Renne. Proc. Natl. Acad. Sci. USA *113*, 11162–11167. https://doi.org/10.1073/pnas.1605834113.
39. Hublin, J.-J., Talamo, S., Julien, M., David, F., Connet, N., Bodu, P., Vandermeersch, B., and Richards, M.P. (2012). Radiocarbon dates from the Grotte du Renne and Saint-Césaire support a Neandertal origin for the Châtelperronian. Proc. Natl. Acad. Sci. USA *109*, 18743–18748. https://doi.org/10.1073/pnas.1212924109.
40. Douka, K., Brown, S., Higham, T., Pääbo, S., Derevianko, A., and Shunkov, M. (2019). FINDER project: collagen fingerprinting (ZooMS) for the identification of new human fossils. Antiquity *93*, e1. https://doi.org/10.15184/aqy.2019.3.
41. Buckley, M., Collins, M., Thomas-Oates, J., and Wilson, J.C. (2009). Species identification by analysis of bone collagen using matrix-assisted laser desorption/ionisation time-of-flight mass spectrometry. Rapid Commun. Mass Spectrom. *23*, 3843–3854. https://doi.org/10.1002/rcm.4316.
42. van der Sluis, L.G., Hollund, H., Buckley, M., De Louw, P., Rijsdijk, K., and Kars, H. (2014). Combining histology, stable isotope analysis and ZooMS collagen fingerprinting to investigate the taphonomic history and dietary behaviour of extinct giant tortoises from the Mare aux Songes deposit on Mauritius. Palaeogeogr. Palaeoclimatol. Palaeoecol. *416*, 80–91. https://doi.org/10.1016/j.palaeo.2014.06.003.
43. Brown, S., Higham, T., Slon, V., Pääbo, S., Meyer, M., Douka, K., Brock, F., Comeskey, D., Procopio, N., Shunkov, M., et al. (2016). Identification of a new hominin bone from Denisova Cave, Siberia using collagen fingerprinting and mitochondrial DNA analysis. Sci. Rep. *6*, 23559. https://doi.org/10.1038/srep23559.
44. Deviese, T., Comeskey, D., McCullagh, J., Ramsey, C.B., and Higham, T. (2018). New protocol for compound specific radiocarbon analysis of archaeological bones. Rapid Commun. Mass Spectrom. *32*, 373–379. https://doi.org/10.1002/rcm.8047.
45. Picin, A., Hajdinjak, M., Nowaczewska, W., Benazzi, S., Urbanowski, M., Marciszak, A., Fewlass, H., Bosch, M.D., Socha, P., Stefaniak, K., et al. (2020). New perspectives on Neanderthal dispersal and turnover from Stajnia Cave (Poland). Sci. Rep. *10*, 14778. https://doi.org/10.1038/s41598-020-71504-x.
46. Reich, D., Green, R.E., Kircher, M., Krause, J., Patterson, N., Durand, E.Y., Viola, B., Briggs, A.W., Stenzel, U., Johnson, P.L.F., et al. (2010). Genetic history of an archaic hominin group from Denisova cave in Siberia. Nature *468*, 1053–1060. https://doi.org/10.1038/nature09710.
47. Bokelmann, L., Hajdinjak, M., Peyrégne, S., Brace, S., Essel, E., de Filippo, C., Glocke, I., Grote, S., Mafessoni, F., Nagel, S., et al. (2019). A genetic analysis of the Gibraltar Neanderthals. Proc. Natl. Acad. Sci. USA *116*, 15610–15615. https://doi.org/10.1073/pnas.1903984116.
48. Skov, L., Peyrégne, S., Popli, D., Iasi, L.N.M., Devièse, T., Slon, V., Zavala, E.I., Hajdinjak, M., Sümer, A.P., Grote, S., et al. (2022). Genetic insights into the social organization of Neanderthals. Nature *610*, 519–525. https://doi.org/10.1038/s41586-022-05283-y.
49. Bouckaert, R., Vaughan, T.G., Barido-Sottani, J., Duchêne, S., Fourment, M., Gavryushkina, A., Heled, J., Jones, G., Kühnert, D., De Maio, N., et al. (2019). BEAST 2.5: An advanced software platform for Bayesian evolutionary analysis. PLoS Comput. Biol. *15*, e1006650. https://doi.org/10.1371/journal.pcbi.1006650.
50. Rieux, A., and Balloux, F. (2016). Inferences from tip-calibrated phylogenies: a review and a practical guide. Mol. Ecol. *25*, 1911–1924. https://doi.org/10.1111/mec.13586.
51. Skinner, A.R., Blackwell, B.A.B., Martin, S., Ortega, A., Blickstein, J.I.B., Golovanova, L.V., and Doronichev, V.B. (2005). ESR dating at Mezmaiskaya Cave, Russia. Appl. Radiat. Isot. *62*, 219–224. https://doi.org/10.1016/j.apradiso.2004.08.008.
52. Skoglund, P., Northoff, B.H., Shunkov, M.V., Derevianko, A.P., Pääbo, S., Krause, J., and Jakobsson, M. (2014). Separating endogenous ancient DNA from modern day contamination in a Siberian Neandertal. Proc. Natl. Acad. Sci. USA *111*, 2229–2234. https://doi.org/10.1073/pnas.1318934111.
53. Meyer, M., Kircher, M., Gansauge, M.T., Li, H., Racimo, F., Mallick, S., Schraiber, J.G., Jay, F., Prüfer, K., de Filippo, C., et al. (2012). A high-coverage genome sequence from an archaic Denisovan individual. Science *338*, 222–226. https://doi.org/10.1126/science.1224344.
54. Kamm, J., Terhorst, J., Durbin, R., and Song, Y.S. (2020). Efficiently Inferring the Demographic History of Many Populations With Allele Count Data. J. Am. Stat. Assoc. *115*, 1472–1487. https://doi.org/10.1080/01621459.2019.1635482.
55. Slimak, L., Lewis, J.E., Crégut-Bonnoure, E., Metz, L., Ollivier, V., André, P., Chrzavzez, J., Giraud, Y., Jeannet, M., and Magnin, F. (2010). Le Grand Abri aux Puces, a Mousterian site from the Last Interglacial: paleogeography, paleoenvironment, and new excavation results. J. Archaeol. Sci. *37*, 2747–2761. https://doi.org/10.1016/j.jas.2010.06.010.
56. Slimak, L., and Nicholson, C. (2020). Cannibals in the forest: A comment on Defleur and Desclaux (2019). J. Archaeol. Sci. *117*, 105034. https://doi.org/10.1016/j.jas.2019.105034.
57. Lévi-Strauss, C. (1949). The Elementary Structures of Kinship (Presses Universitaires de France).
58. Combier, J. (1967). Le Paléolithique de L'Ardeche dans son Cadre Paléoclimatique (Imprimeries Delmas).
59. Andrews, R.M., Kubacka, I., Chinnery, P.F., Lightowlers, R.N., Turnbull, D.M., and Howell, N. (1999). Reanalysis and revision of the Cambridge reference sequence for human mitochondrial DNA. Nat. Genet. *23*, 147. https://doi.org/10.1038/13779.
60. Mallick, S., Micco, A., Mah, M., Ringbauer, H., Lazaridis, I., Olalde, I., Patterson, N., and Reich, D. (2024). The Allen Ancient DNA Resource (AADR) a curated compendium of ancient human genomes. Sci. Data *11*, 182. https://doi.org/10.1038/s41597-024-03031-7.
61. 1000 Genomes Project Consortium; Abecasis, G.R., Altshuler, D., Auton, A., Brooks, L.D., Durbin, R.M., Gibbs, R.A., Hurles, M.E., and McVean, G.A. (2010). A map of human genome variation from population-scale sequencing. Nature *467*, 1061–1073. https://doi.org/10.1038/nature09534.
62. Paton, C., Hellstrom, J., Paul, B., Woodhead, J., and Hergt, J. (2011). Iolite: Freeware for the visualisation and processing of mass spectrometric data. J. Anal. At. Spectrom. *26*, 2508–2518. https://doi.org/10.1039/C1JA10172B.
63. Joannes-Boyau, R., Duval, M., and Bodin, T. (2018). MCDoseE 2.0. A new Markov Chain Monte Carlo program for ESR dose response curve fitting and dose evaluation. Quat. Geochronol. *44*, 13–22. https://doi.org/10.1016/j.quageo.2017.11.003.
64. Bronk Ramsey, C. (2009). Bayesian analysis of radiocarbon dates. Radiocarbon *51*, 337–360. https://doi.org/10.1017/S0033822200033865.
65. Schubert, M., Ermini, L., Der Sarkissian, C., Jónsson, H., Ginolhac, A., Schaefer, R., Martin, M.D., Fernández, R., Kircher, M., McCue, M., et al. (2014). Characterization of ancient and modern genomes by SNP detection and phylogenomic and metagenomic analysis using PALEOMIX. Nat. Protoc. *9*, 1056–1082. https://doi.org/10.1038/nprot.2014.063.
66. Lindgreen, S. (2012). AdapterRemoval: Easy cleaning of next-generation sequencing reads. BMC Res. Notes *5*, 337. https://doi.org/10.1186/1756-0500-5-337.
67. Li, H., and Durbin, R. (2009). Fast and accurate short read alignment with Burrows-Wheeler transform. Bioinformatics *25*, 1754–1760. https://doi.org/10.1093/bioinformatics/btp324.
68. McKenna, A., Hanna, M., Banks, E., Sivachenko, A., Cibulskis, K., Kernytsky, A., Garimella, K., Altshuler, D., Gabriel, S., Daly, M., and DePristo, M.A. (2010). The Genome Analysis Toolkit: A MapReduce framework for

analyzing next-generation DNA sequencing data. Genome Res. *20*, 1297–1303. https://doi.org/10.1101/gr.107524.110.

69. Li, H., Handsaker, B., Wysoker, A., Fennell, T., Ruan, J., Homer, N., Marth, G., Abecasis, G., and Durbin, R.; 1000 Genome Project Data Processing Subgroup (2009). The Sequence Alignment/Map format and SAMtools. Bioinformatics *25*, 2078–2079. https://doi.org/10.1093/bioinformatics/btp352.
70. Jónsson, H., Ginolhac, A., Schubert, M., Johnson, P.L.F., and Orlando, L. (2013). mapDamage2.0: Fast approximate Bayesian estimates of ancient DNA damage parameters. Bioinformatics *29*, 1682–1684. https://doi.org/10.1093/bioinformatics/btt193.
71. Al-Asadi, H., Dey, K.K., Novembre, J., and Stephens, M. (2019). Inference and visualization of DNA damage patterns using a grade of membership model. Bioinformatics *35*, 1292–1298. https://doi.org/10.1093/bioinformatics/bty779.
72. Korneliussen, T.S., Albrechtsen, A., and Nielsen, R. (2014). ANGSD: Analysis of Next Generation Sequencing Data. BMC Bioinf. *15*, 356. https://doi.org/10.1186/s12859-014-0356-4.
73. Fu, Q., Mittnik, A., Johnson, P.L.F., Bos, K., Lari, M., Bollongino, R., Sun, C., Giemsch, L., Schmitz, R., Burger, J., et al. (2013). A revised timescale for human evolution based on ancient mitochondrial genomes. Curr. Biol. *23*, 553–559. https://doi.org/10.1016/j.cub.2013.02.044.
74. Li, H. (2011). A statistical framework for SNP calling, mutation discovery, association mapping and population genetical parameter estimation from sequencing data. Bioinformatics *27*, 2987–2993. https://doi.org/10.1093/bioinformatics/btr509.
75. Katoh, K., and Standley, D.M. (2013). MAFFT multiple sequence alignment software version 7: Improvements in performance and usability. Mol. Biol. Evol. *30*, 772–780. https://doi.org/10.1093/molbev/mst010.
76. Breitwieser, F.P., Baker, D.N., and Salzberg, S.L. (2018). KrakenUniq: confident and fast metagenomics classification using unique k-mer counts. Genome Biol. *19*, 198. https://doi.org/10.1186/s13059-018-1568-0.
77. Kozlov, A.M., Darriba, D., Flouri, T., Morel, B., and Stamatakis, A. (2019). RAxML-NG: A fast, scalable, and user-friendly tool for maximum likelihood phylogenetic inference. Bioinformatics *35*, 4453–4455. https://doi.org/10.1093/bioinformatics/btz305.
78. Schliep, K.P. (2011). Phangorn: phylogenetic analysis in R. Bioinformatics *27*, 592–593. https://doi.org/10.1093/bioinformatics/btq706.
79. Bouckaert, R.R., and Drummond, A.J. (2017). bModelTest: Bayesian phylogenetic site model averaging and model comparison. BMC Evol. Biol. *17*, 42. https://doi.org/10.1186/s12862-017-0890-6.
80. Purcell, S., Neale, B., Todd-Brown, K., Thomas, L., Ferreira, M.A.R., Bender, D., Maller, J., Sklar, P., de Bakker, P.I.W., Daly, M.J., and Sham, P.C. (2007). PLINK: A tool set for whole-genome association and population-based linkage analyses. Am. J. Hum. Genet. *81*, 559–575. https://doi.org/10.1086/519795.
81. Patterson, N., Price, A.L., and Reich, D. (2006). Population structure and eigenanalysis. PLoS Genet. *2*, e190–e2093. https://doi.org/10.1371/journal.pgen.0020190.
82. Oksanen, J., Simpson, G.L., Blanchet, F.G., Kindt, R., Legendre, P., Minchin, P.R., O'Hara, R.B., Solymos, P., Stevens, M.H.H., Szoecs, E., et al. (2019). Vegan: Community Ecology Package. R package version 2.5-4.
83. Pickrell, J.K., and Pritchard, J.K. (2012). Inference of Population Splits and Mixtures from Genome-Wide Allele Frequency Data. PLoS Genet. *8*, 1002967. https://doi.org/10.1371/journal.pgen.1002967.
84. Arnold, T.B., and Tibshirani, R.J. (2016). Efficient Implementations of the Generalized Lasso Dual Path Algorithm. J. Comput. Graph Stat. *25*, 1–27. https://doi.org/10.1080/10618600.2015.1008638.
85. Buckley, M., and Kansa, S.W. (2011). Collagen fingerprinting of archaeological bone and teeth remains from Domuztepe, South Eastern Turkey. Archaeol. Anthropol. Sci. *3*, 271–280. https://doi.org/10.1007/s12520-011-0066-z.
86. Dee, M., and Bronk Ramsey, C. (2000). Refinement of Graphite Target Production at ORAU. Nucl. Instrum. Methods Phys. Res. B *172*, 449–453. https://doi.org/10.1016/S0168-583X(00)00337-2.
87. Joannes-Boyau, R., Grün, R., and Grün, R. (2010). Decomposition of the laboratory gamma irradiation component of angular ESR spectra of fossil tooth enamel fragments. Appl. Radiat. Isot. *68*, 1798–1808. https://doi.org/10.1016/j.apradiso.2010.03.015.
88. Joannes-Boyau, R., and Grün, R. (2011). A comprehensive model for CO_2^- radicals in fossil tooth enamel: Implications for ESR dating. Quat. Geochronol. *6*, 82–97. https://doi.org/10.1016/j.quageo.2010.09.001.
89. Joannes-Boyau, R. (2013). Detailed protocol for an accurate non-destructive direct dating of tooth enamel fragment using Electron Spin Resonance. Geochronometria *40*, 322–333. https://doi.org/10.2478/s13386-013-0132-7.
90. Grün, R., Mahat, R., and Joannes-Boyau, R. (2012). Ionization efficiencies of alanine dosimeters and tooth enamel irradiated by gamma and X-ray sources. Rad. Meas. *47*, 665–668. https://doi.org/10.1016/J.RADMEAS.2012.03.018.
91. Joannes-Boyau, R., and Grün, R. (2009). Thermal behavior of orientated and non-orientated CO_2^- radicals in tooth enamel. Rad. Meas. *44*, 505–511. https://doi.org/10.1016/j.radmeas.2009.02.010.
92. Reimer, P.J., Austin, W.E.N., Bard, E., Bayliss, A., Blackwell, P.G., Bronk Ramsey, C., Butzin, M., Cheng, H., Edwards, R.L., Friedrich, M., et al. (2020). The IntCal20 Northern Hemisphere radiocarbon age calibration curve (0–55 cal kBP). Radiocarbon *62*, 725–757. https://doi.org/10.1017/RDC.2020.41.
93. Bronk Ramsey, C. (2009). Dealing with outliers and offsets in radiocarbon dating. Radiocarbon *51*, 1023–1045. https://doi.org/10.1017/S0033822200034093.
94. Koch, P.L. (2007). Isotopic study of the biology of modern and fossil vertebrates. In Stable Isotopes in Ecology and Environmental Science 2, R. Michener and K. Kajtha, eds., pp. 99–154. https://doi.org/10.1002/9780470691854.ch5.
95. Bocherens, H., and Drucker, D.G. (2013). Terrestrial teeth and bones. In Encyclopedia of Quaternary Sciences, 2nd Edition vol. 1, S.A. Elias, ed. (Amsterdam: Elsevier), pp. 304–314. https://doi.org/10.1016/B0-444-52747-8/00353-7.
96. Ecker, M., Bocherens, H., Julien, M.A., Rivals, F., Raynal, J.P., and Moncel, M.H. (2013). Middle Pleistocene ecology and Neanderthal subsistence: insights from stable isotope analyses in Payre (Ardèche, southeastern France). J. Hum. Evol. *65*, 363–373. https://doi.org/10.1016/j.jhevol.2013.06.013.
97. Bocherens, H., Díaz-Zorita Bonilla, M., Daujeard, C., Fernandes, P., Raynal, J.-P., and Moncel, M.H. (2016). Direct isotopic evidence for subsistence variability in Middle Pleistocene Neanderthals (Payre, southeastern France). Quat. Sci. Rev. *154*, 226–236. https://doi.org/10.1016/j.quascirev.2016.11.004.
98. Moncel, M.-H., Fernandes, P., Willmes, M., James, H., and Grün, R. (2019). Rocks, teeth, and tools: New insights into early Neanderthal mobility strategies in South-Eastern France from lithic reconstructions and strontium isotope analysis. PLoS One *14*, e0214925. https://doi.org/10.1371/journal.pone.0214925.
99. Bocherens, H., Fizet, M., and Mariotti, A. (1994). Diet, physiology and ecology of fossil mammals as inferred from stable carbon and nitrogen isotope biogeochemistry: implications for Pleistocene bears. Palaeogeogr. Palaeoclimatol. Palaeoecol. *107*, 213–225. https://doi.org/10.1016/0031-0182(94)90095-7.
100. Bon, C., Berthonaud, V., Fosse, P., Gély, B., Maksud, F., Vitalis, R., Philippe, M., van der Plicht, J., and Elalouf, J.M. (2011). Low regional diversity of late cave bears mitochondrial DNA at the time of Chauvet Aurignacian paintings. J. Archaeol. Sci. *38*, 1886–1895. https://doi.org/10.1016/j.jas.2011.03.033.

101. Szmidt, C.C., Moncel, M.-H., and Daujeard, C. (2010). New data on the Late Mousterian in Mediterranean France: First radiocarbon (AMS) dates at Saint-Marcel Cave (Ardèche). C. R. Palevol *9*, 185–199. https://doi.org/10.1016/j.crpv.2010.05.002.

102. Szmidt, C.C., Brou, L., and Jaccottey, L. (2010). Direct radiocarbon (AMS) dating of split-based points from the (Proto)Aurignacian of Trou de la Mère Clochette, Northeastern France. Implications for the characterization of the Aurignacian and the timing of technical innovations in Europe. J. Archaeol. Sci. *37*, 3320–3337. https://doi.org/10.1016/j.jas.2010.08.001.

103. Daujeard, C., Vettese, D., Britton, K., Béarez, P., Boulbes, N., Crégut-Bonnoure, E., Desclaux, E., Lateur, N., Pike-Tay, A., Rivals, F., et al. (2019). Neanderthal selective hunting of reindeer? The case study of Abri du Maras (south-eastern France). Archaeol. Anthropol. Sci. *11*, 985–1011. https://doi.org/10.1007/s12520-017-0580-8.

104. Garcia, N., Feranec, R.S., Passey, B.H., Cerling, T.E., and Arsuaga, J.L. (2015). Exploring the potential of laser ablation carbon isotope analysis for examining ecology during the ontogeny of Middle Pleistocene Hominins from Sima de los Huesos (Northern Spain). PLoS One *10*, e0142895. https://doi.org/10.1371/journal.pone.0142895.

105. Knipper, C., Pichler, S.L., Brönnimann, D., Rissanen, H., Rosner, M., Spichtig, N., Stopp, B., Rentzel, P., Röder, B., Schibler, J., et al. (2018). A knot in a network: Residential mobility at the Late Iron Age proto-urban centre of Basel-Gasfabrik (Switzerland) revealed by isotope analyses. J. Archaeol. Sci. Rep *17*, 735–753. https://doi.org/10.1016/j.jasrep.2017.12.001.

106. Bocherens, H., Billiou, D., Patou-Mathis, M., Bonjean, D., Otte, M., and Mariotti, A. (1997). Paleobiological implications of the isotopic signatures (^{13}C, ^{15}N) of fossil mammal collagen in Scladina Cave (Sclayn, Belgium). Quat. Res. *48*, 370–380. https://doi.org/10.1006/qres.1997.1927.

107. DeNiro, M.J. (1985). Postmortem preservation and alteration of in vivo bone collagen isotope ratios in relation to palaeodietary reconstruction. Nature *317*, 806–809. https://doi.org/10.1038/317806a0.

108. Van Klinken, G.J. (1999). Bone collagen quality indicators for palaeodietary and radiocarbon measurements. J. Archaeol. Sci. *26*, 687–695. https://doi.org/10.1006/jasc.1998.0385.

109. Wißing, C., Rougier, H., Crevecoeur, I., Germonpré, M., Naito, Y.I., Semal, P., and Bocherens, H. (2016). Isotopic evidence for dietary ecology of late Neandertals in North-Western Europe. Quat. Int. *411*, 327–345. https://doi.org/10.1016/j.quaint.2015.09.091.

110. Bocherens, H., Drucker, D.G., Billiou, D., Patou-Mathis, M., and Vandermeersch, B. (2005). Isotopic evidence for diet and subsistence pattern of the Saint-Césaire I Neanderthal: Review and use of a multi-source mixing model. J. Hum. Evol. *49*, 71–87. https://doi.org/10.1016/j.jhevol.2005.03.003.

111. Bocherens, H., Drucker, D.G., and Madelaine, S. (2014). Evidence for a ^{15}N positive excursion in terrestrial foodwebs at the middle to upper Palaeolithic transition in South-western France: implication for early modern human palaeodiet and palaeoenvironment. J. Hum. Evol. *69*, 31–43. https://doi.org/10.1016/j.jhevol.2013.12.015.

112. Rohland, N., Harney, E., Mallick, S., Nordenfelt, S., and Reich, D. (2015). Partial uracil-DNA-glycosylase treatment for screening of ancient DNA. Philos. Trans. R. Soc. Lond. B Biol. Sci. *370*, 20130624. https://doi.org/10.1098/rstb.2013.0624.

113. Enk, J.M., Devault, A.M., Kuch, M., Murgha, Y.E., Rouillard, J.M., and Poinar, H.N. (2014). Ancient whole genome enrichment using baits built from modern DNA. Mol. Biol. Evol. *31*, 1292–1294. https://doi.org/10.1093/molbev/msu074.

114. Meyer, M., and Kircher, M. (2010). Illumina sequencing library preparation for highly multiplexed target capture and sequencing. Cold Spring Harb. Protoc. *2010*, pdb.prot5448. https://doi.org/10.1101/pdb.prot5448.

115. Sikora, M., Pitulko, V.V., Sousa, V.C., Allentoft, M.E., Vinner, L., Rasmussen, S., Margaryan, A., de Barros Damgaard, P., de la Fuente, C., Renaud, G., et al. (2019). The population history of northeastern Siberia since the Pleistocene. Nature *570*, 182–188. https://doi.org/10.1038/s41586-019-1279-z.

116. Broushaki, F., Thomas, M.G., Link, V., López, S., van Dorp, L., Kirsanow, K., Hofmanová, Z., Diekmann, Y., Cassidy, L.M., Díez-Del-Molino, D., et al. (2016). Early Neolithic genomes from the eastern Fertile Crescent. Science *353*, 499–503. https://doi.org/10.1126/science.aaf7943.

117. Hofmanová, Z., Kreutzer, S., Hellenthal, G., Sell, C., Diekmann, Y., Díez-Del-Molino, D., van Dorp, L., López, S., Kousathanas, A., Link, V., et al. (2016). Early farmers from across Europe directly descended from Neolithic Aegeans. Proc. Natl. Acad. Sci. USA *113*, 6886–6891. https://doi.org/10.1073/pnas.1523951113.

118. Jones, E.R., Gonzalez-Fortes, G., Connell, S., Siska, V., Eriksson, A., Martiniano, R., McLaughlin, R.L., Gallego Llorente, M., Cassidy, L.M., Gamba, C., et al. (2015). Upper Palaeolithic genomes reveal deep roots of modern Eurasians. Nat. Commun. *6*, 8912–8918. https://doi.org/10.1038/ncomms9912.

119. Lazaridis, I., Patterson, N., Mittnik, A., Renaud, G., Mallick, S., Kirsanow, K., Sudmant, P.H., Schraiber, J.G., Castellano, S., Lipson, M., et al. (2014). Ancient human genomes suggest three ancestral populations for present-day Europeans. Nature *513*, 409–413. https://doi.org/10.1038/nature13673.

120. de Barros Damgaard, P., Martiniano, R., Kamm, J., Moreno-Mayar, J.V., Kroonen, G., Peyrot, M., Barjamovic, G., Rasmussen, S., Zacho, C., Baimukhanov, N., et al. (2018). The first horse herders and the impact of early Bronze Age steppe expansions into Asia. Science *360*, eaar7711. https://doi.org/10.1126/science.aar7711.

121. Fu, Q., Li, H., Moorjani, P., Jay, F., Slepchenko, S.M., Bondarev, A.A., Johnson, P.L.F., Aximu-Petri, A., Prüfer, K., de Filippo, C., et al. (2014). Genome sequence of a 45,000-year-old modern human from western Siberia. Nature *514*, 445–449. https://doi.org/10.1038/nature13810.

122. Moreno-Mayar, J.V., Potter, B.A., Vinner, L., Steinrücken, M., Rasmussen, S., Terhorst, J., Kamm, J.A., Albrechtsen, A., Malaspinas, A.S., Sikora, M., et al. (2018). Terminal Pleistocene Alaskan genome reveals first founding population of Native Americans. Nature *553*, 203–207. https://doi.org/10.1038/nature25173.

123. Slon, V., Mafessoni, F., Vernot, B., de Filippo, C., Grote, S., Viola, B., Hajdinjak, M., Peyrégne, S., Nagel, S., Brown, S., et al. (2018). The genome of the offspring of a Neanderthal mother and a Denisovan father. Nature *561*, 113–116. https://doi.org/10.1038/s41586-018-0455-x.

124. Mallick, S., Li, H., Lipson, M., Mathieson, I., Gymrek, M., Racimo, F., Zhao, M., Chennagiri, N., Nordenfelt, S., Tandon, A., et al. (2016). The Simons Genome Diversity Project: 300 genomes from 142 diverse populations. Nature *538*, 201–206. https://doi.org/10.1038/nature18964.

125. Krause, J., Briggs, A.W., Kircher, M., Maricic, T., Zwyns, N., Derevianko, A., and Pääbo, S. (2010). A Complete mtDNA Genome of an Early Modern Human from Kostenki, Russia. Curr. Biol. *20*, 231–236. https://doi.org/10.1016/j.cub.2009.11.068.

126. Posth, C., Renaud, G., Mittnik, A., Drucker, D.G., Rougier, H., Cupillard, C., Valentin, F., Thevenet, C., Furtwängler, A., Wißing, C., et al. (2016). Pleistocene mitochondrial genomes suggest a single major dispersal of non-africans and a late glacial population turnover in Europe. Curr. Biol. *26*, 827–833. https://doi.org/10.1016/j.cub.2016.01.037.

127. Posth, C., Wißing, C., Kitagawa, K., Pagani, L., van Holstein, L., Racimo, F., Wehrberger, K., Conard, N.J., Kind, C.J., Bocherens, H., and Krause, J. (2017). Deeply divergent archaic mitochondrial genome provides lower time boundary for African gene flow into Neanderthals. Nat. Commun. *8*, 16046. https://doi.org/10.1038/ncomms16046.

128. Gansauge, M.T., and Meyer, M. (2014). Selective enrichment of damaged DNA molecules for ancient genome sequencing. Genome Res. *24*, 1543–1549. https://doi.org/10.1101/gr.174201.114.

129. Briggs, A.W., Good, J.M., Green, R.E., Krause, J., Maricic, T., Stenzel, U., Lalueza-Fox, C., Rudan, P., Brajkovic, D., Kucan, Z., et al. (2009).

Targeted retrieval and analysis of five neandertal mtDNA genomes. Science *325*, 318–321. https://doi.org/10.1126/science.1174462.

130. Meyer, M., Arsuaga, J.L., de Filippo, C., Nagel, S., Aximu-Petri, A., Nickel, B., Martínez, I., Gracia, A., Bermúdez de Castro, J.M., Carbonell, E., et al. (2016). Nuclear DNA sequences from the Middle Pleistocene Sima de los Huesos hominins. Nature *531*, 504–507. https://doi.org/10.1038/nature17405.

131. Slon, V., Hopfe, C., Weiß, C.L., Mafessoni, F., de la Rasilla, M., Lalueza-Fox, C., Rosas, A., Soressi, M., Knul, M.V., Miller, R., et al. (2017). Neandertal and Denisovan DNA from Pleistocene sediments. Science *356*, 605–608. https://doi.org/10.1126/science.aam969.

132. Sawyer, S., Renaud, G., Viola, B., Hublin, J.J., Gansauge, M.T., Shunkov, M.V., Derevianko, A.P., Prüfer, K., Kelso, J., and Pääbo, S. (2015). Nuclear and mitochondrial DNA sequences from two Denisovan individuals. Proc. Natl. Acad. Sci. USA *112*, 15696–15700. https://doi.org/10.1073/pnas.1519905112.

133. Slon, V., Viola, B., Renaud, G., Gansauge, M.T., Benazzi, S., Sawyer, S., Hublin, J.J., Shunkov, M.V., Derevianko, A.P., Kelso, J., et al. (2017). A fourth Denisovan individual. Sci. Adv. *3*, e1700186. https://doi.org/10.1126/sciadv.1700186.

134. Fu, Q., Meyer, M., Gao, X., Stenzel, U., Burbano, H.A., Kelso, J., and Pääbo, S. (2013). DNA analysis of an early modern human from Tianyuan Cave, China. Proc. Natl. Acad. Sci. USA *110*, 2223–2227. https://doi.org/10.1073/pnas.1221359110.

135. Krause, J., Fu, Q., Good, J.M., Viola, B., Shunkov, M.V., Derevianko, A.P., and Pääbo, S. (2010). The complete mitochondrial DNA genome of an unknown hominin from southern Siberia. Nature *464*, 894–897. https://doi.org/10.1038/nature08976.

136. Ingman, M., Kaessmann, H., Pääbo, S., and Gyllensten, U. (2001). Erratum: correction: Mitochondrial genome variation and the origin of modern humans. Nature *410*, 611. https://doi.org/10.1038/35047064.

137. Tamura, K., and Nei, M. (1993). Estimation of the number of nucleotide substitutions in the control region of mitochondrial DNA in humans and chimpanzees. Mol. Biol. Evol. *10*, 512–526. https://doi.org/10.1093/oxfordjournals.molbev.a040023.

138. Gamba, C., Jones, E.R., Teasdale, M.D., McLaughlin, R.L., Gonzalez-Fortes, G., Mattiangeli, V., Domboróczki, L., Kővári, I., Pap, I., Anders, A., et al. (2014). Genome flux and stasis in a five millennium transect of European prehistory. Nat. Commun. *5*, 5257. https://doi.org/10.1038/ncomms6257.

139. Skoglund, P., Malmström, H., Raghavan, M., Storå, J., Hall, P., Willerslev, E., Gilbert, M.T.P., Götherström, A., and Jakobsson, M. (2012). Origins and Genetic Legacy of Neolithic Farmers and Hunter-Gatherers in Europe. Science *336*, 466–469. https://doi.org/10.1126/science.121630.

140. Maier, R., Flegontov, P., Flegontova, O., Işıldak, U., Changmai, P., and Reich, D. (2023). On the limits of fitting complex models of population history to *f*-statistics. Elife *12*, e85492. https://doi.org/10.7554/eLife.85492.

141. Tibshirani, R., Saunders, M., Rosset, S., Zhu, J., and Knight, K. (2005). Sparsity and smoothness via the fused lasso. J. Royal Stat. Soc. B. *67*, 91–108. https://doi.org/10.1111/j.1467-9868.2005.00490.x.

STAR★METHODS

KEY RESOURCES TABLE

REAGENT or RESOURCE	SOURCE	IDENTIFIER
Biological samples		
Thorin tooth for genomic analyses	This study	MAN-15-B2-1600, CGG_2_016357
Thorin bone fragment for HYP dating	This study	OxA-37787
Thorin bone fragment for HYP dating	This study	OxA-38388
Thorin bone fragment for HYP dating	This study	OxA-38389
Thorin tooth for U-series dating	This study	GM-BP-SCU1
Thorin tooth dentine for isotopic analyses	This study	GM-35
Bison premolar layer B2 for U-series dating	This study	GM-BP-SCU2
Caprinid molar layer B3 for U-series dating	This study	1996-E0-B#65
Hippopotamus tooth for dating calibration	This study	SCU-14033-KR
Neolithic Homo sapiens tooth layer A for isotopic analyses	This study	GM-1
Neolithic Homo sapiens tooth layer A for isotopic analyses	This study	GM-2
Bison priscus tooth layer B for isotopic analyses	This study	GM-3
Bison priscus tooth layer B for isotopic analyses	This study	GM-4
Bison priscus tooth layer B2 for isotopic analyses	This study	GM-11
cf. Bison priscus tooth layer C for isotopic analyses	This study	GM-29
Bison priscus tooth layer C for isotopic analyses	This study	GM-30
Cervus elaphus tooth layer B for isotopic analyses	This study	GM-6
Cervus elaphus tooth layer B for isotopic analyses	This study	GM-8
Cervus elaphus tooth layer C for isotopic analyses	This study	GM-31
Cervus elaphus tooth layer C for isotopic analyses	This study	GM-32
Cervus elaphus tooth layer B2 for isotopic analyses	This study	GM-17
Cervus elaphus tooth layer B2 for isotopic analyses	This study	GM-18
Rangifer tarandus tooth layer B2 for isotopic analyses	This study	GM-21
Rangifer tarandus tooth layer B2 for isotopic analyses	This study	GM-22
Rangifer tarandus tooth layer B2 for isotopic analyses	This study	GM-23
Equus cf. germanicus tooth layer B2 for isotopic analyses	This study	GM-24
Equus cf. germanicus tooth layer B2 for isotopic analyses	This study	GM-26
Equus cf. germanicus tooth layer B2 for isotopic analyses	This study	GM-27
Equus cf. germanicus tooth layer B2 for isotopic analyses	This study	GM-28
Unidentified bone fragment for ZooMS analysis	This study	1577
Unidentified bone fragment for ZooMS analysis	This study	2200
Unidentified bone fragment for ZooMS analysis	This study	2853
Unidentified bone fragment for ZooMS analysis	This study	1574
Unidentified bone fragment for ZooMS analysis	This study	1265
Unidentified bone fragment for ZooMS analysis	This study	1618
Unidentified bone fragment for ZooMS analysis	This study	1590
Unidentified bone fragment for ZooMS analysis	This study	1279
Unidentified bone fragment for ZooMS analysis	This study	1275

(*Continued on next page*)

Continued

REAGENT or RESOURCE	SOURCE	IDENTIFIER
Unidentified bone fragment for ZooMS analysis	This study	1615
Unidentified bone fragment for ZooMS analysis	This study	2854
Unidentified bone fragment for ZooMS analysis	This study	1614
Unidentified bone fragment for ZooMS analysis	This study	1341
Unidentified bone fragment for ZooMS analysis	This study	1597
Unidentified bone fragment for ZooMS analysis	This study	556
Unidentified bone fragment for ZooMS analysis	This study	1575
Unidentified bone fragment for ZooMS analysis	This study	2855A
Unidentified bone fragment for ZooMS analysis	This study	2855B
Unidentified bone fragment for ZooMS analysis	This study	1272
Unidentified bone fragment for ZooMS analysis	This study	1602
Unidentified bone fragment for ZooMS analysis	This study	1504
Unidentified bone fragment for ZooMS analysis	This study	1161
Unidentified bone fragment for ZooMS analysis	This study	1920
Unidentified bone fragment for ZooMS analysis	This study	1502
Unidentified bone fragment for ZooMS analysis	This study	1596
Unidentified bone fragment for ZooMS analysis	This study	1587B
Unidentified bone fragment for ZooMS analysis	This study	1587A
Unidentified bone fragment for ZooMS analysis	This study	1576
Unidentified bone fragment for ZooMS analysis	This study	1583
Unidentified bone fragment for ZooMS analysis	This study	3299
Chemicals, peptides, and recombinant proteins		
Proteinase K	Sigma-Aldrich	Cat#3115844001
Dynabeads™ MyOne™ Streptavidin C1 beads	Invitrogen	Cat#10099482
HiFi HotStart Uracil+ ReadyMix	KAPA Biosystems, Inc.	Cat#KK2801
AmpliTaq Gold	Applied Biosystems	Cat#N8080241
Critical commercial assays		
MinElute PCR Purification Kit	QIAGEN	Cat#28006
NEBNext DNA Sample Prep Master Mix Set 2	New England Biolabs Inc.	Cat#E6070
OMIX, C18	Varian	Cat#VARIA5700310
Amicon Ultra-4 30kD	Millipore	Cat#UFC803024
Uracil-Specific Excision Reagent	New England Biolabs Inc.	Cat#M5505
Kapa Library Quantification Kit Illumina	KapaBiosystems	Cat#KK4854
HiSeq SBS Kit v4 (250 Cycle)	Illumina	Cat#FC-401-4003
HiSeq SR Cluster Kit v4 – cBot™ - HS	Illumina	Cat#GD-401-4001
HiSeq PE Cluster Kit v4 – cBot™ - HS	Illumina	Cat#PE-401-4001
MYBaits WGE kit v2	MYcroarray-Daicel Arbor Biosciences	Cat#MYbaits-WGE-48
Deposited data		
Whole genome sequencing of the Thorin specimen	This study	ENA project PRJEB73284
Human reference genome hg19	Genome Reference Consortium	https://www.ncbi.nlm.nih.gov/datasets/genome/GCF_000001405.13/
revised Cambridge reference mitochondrial sequence (rCRS)	Andrews et al.[59]	GenBank NC_012920.1
Ancient genomes: Allen Ancient DNA Resource (AADR)	Mallick et al.[60]	https://doi.org/10.7910/DVN/FFIDCW
Modern genomes	The 1000 Genomes Project Consortium[61]	https://www.internationalgenome.org/
Sediment samples for DNA analysis	Vernot et al.[14]	ENA project PRJEB42656

(*Continued on next page*)

Continued

REAGENT or RESOURCE	SOURCE	IDENTIFIER
Software and algorithms		
Iolite™	Paton et al.[62]	https://iolite.xyz/
McDoseE 2.0	Joannes-Boyau et al.[63]	https://doi.org/10.1016/j.quageo.2017.11.003
OxCal 4.4	Bronk Ramsey[64]	https://c14.arch.ox.ac.uk/oxcal
IonOS v 3.2	elementar	https://www.elementar.com/fr/
CASAVA	Illumina	v.1.8.2
PALEOMIX v1.1.1	Schubert et al.[65]	https://github.com/MikkelSchubert/paleomix/tree/master/paleomix
AdapterRemoval	Lindgreen[66]	https://adapterremoval.readthedocs.io/en/stable/index.html
BWA 0.5.9-r26-dev	Li and Durbin[67]	http://bio-bwa.sourceforge.net/
GATK	McKenna et al.[68]	https://gatk.broadinstitute.org/hc/en-us
SAMtools v. 1.3.1	Li et al.[69]	http://www.htslib.org/
mapDamage 2.0	Jónsson et al.[70]	https://ginolhac.github.io/mapDamage/
aRchaic	Al-Asadi et al.[71]	https://kkdey.github.io/aRchaic/articles/archaic.html
ANGSD	Korneliussen et al.[72]	http://www.popgen.dk/angsd/index.php/ANGSD
contaMix	Fu et al.[73]	https://www.cell.com/cms/10.1016/j.cub.2013.02.044/attachment/6a56a4c2-3a69-477f-9ceb-06405257545d/mmc1.pdf
BCFtools v.1.10.2	Li[74]	https://github.com/samtools/bcftools
MAFFT	Katoh et al.[75]	https://mafft.cbrc.jp/alignment/software/
KrakenUniq v. 0.5.8	Breitwieser et al.[76]	https://github.com/fbreitwieser/krakenuniq
RaxML-NG	Kozlov et al.[77]	https://github.com/amkozlov/raxml-ng
phangorn	Schliep[78]	https://klausvigo.github.io/phangorn/
BEAST v. 2.6.3	Bouckaert et al.[49]	https://www.beast2.org/
bModelTest	Bouckaert and Drummond[79]	https://github.com/BEAST2-Dev/bModelTest
PLINK v. 1.9	Purcell et al.[80]	https://zzz.bwh.harvard.edu/plink/plink2.shtml
EIGENSOFT	Patterson et al.[81]	https://github.com/DReichLab/EIG
vegan	Oksanen et al.[82]	https://cran.r-project.org/src/contrib/Archive/vegan/
ADMIXTOOLS 2.0	Maier et al.[81]	https://uqrmaie1.github.io/admixtools/
Treemix	Pickrell and Pritchard[83]	https://bitbucket.org/nygcresearch/treemix/wiki/Home
genlasso v. 1.6.1	Arnold and Tibshirani[84]	https://cran.r-project.org/web/packages/genlasso/index.html
momi2	Kamm et al.[54]	https://github.com/popgenmethods/momi2
Other		
Phoenix Nanotom 180 - GE Sensing	Waygate Technologies	https://www.bakerhughes.com/fr/waygate-technologies
Phoenix GE v|tome|x s	Waygate Technologies	https://www.bakerhughes.com/fr/waygate-technologies
Ultraflex II MALDI TOF Mass Spectrometer	Bruker	https://www.bruker.com/fr.html
213 nm laser NWR	Elemental Scientific Lasers	https://www.icpmslasers.com/products/esl213/
Neptune XT multi-collector ICP-MS	ThermoFisher	https://www.thermofisher.com/order/catalog/product/IQLAAEGAASFADOMAJL?SID=srch-srp-IQLAAEGAASFADOMAJL

(*Continued on next page*)

Continued

REAGENT or RESOURCE	SOURCE	IDENTIFIER
MS5000 ESR X-band spectrometer	Freiberg instruments	https://www.bruker.com/en/products-and-solutions/mr/epr-instruments/magnettechesr5000.html
VF50 X-ray gun	Varex	https://www.vareximaging.com/solutions/vf-50-ux/
ProStar high-performance liquid chromatography (HPLC) system	Varian Analytical Instruments, Walnut Creek, CA, USA	ProStar
PDZ-Europa Robo-Prep combustion elemental analyzer/PDZ-Europa 20/20 mass spectrometer	Sercon UK	https://sercon-instruments.com/
MultiFlow-Geo interfaced with IsoPrime 100 IRMS	Elementar	https://www.elementar.com/fr/
Mass Spectrometer HR-MC-ICP MS, Neptune	ThermoFisher	https://www.thermofisher.com/search/browse/category/us/fr/90207133
Thermo Scientific Flash1112	ThermoFisher	https://www.thermofisher.com/fr/fr/home.html
Thermo Delta V Advantage mass spectrometer	ThermoFisher	https://www.thermofisher.com/fr/fr/home.html
TapeStation 2200	Agilent	Cat#G2964AA
HiSeq2500	Illumina	https://support.illumina.com/sequencing/sequencing_instruments/hiseq_2500.html
OSL sediment sample from Level B2	Slimak et al.[1]	Lab ID X6717

RESOURCE AVAILABILITY

Lead contact

Further information and requests for resources and reagents should be directed to and will be fulfilled by the lead contact, Martin Sikora (martin.sikora@sund.ku.dk).

Materials availability

This study did not generate new unique reagents.

Data and code availability

- Genomic data have been deposited at the European Nucleotide Archive (ENA) and are publicly available as of the date of publication. Accession number is listed in the key resources table. This paper analyzes existing, publicly available data. These accession numbers or links for the datasets are listed in the key resources table. Paleoproteomic data are freely available as raw files on FigShare: https://doi.org/10.6084/m9.figshare.16676839.
- This paper does not report original code except for the Bayesian Model CQL code for Thorin age reported in the STAR Methods section. The published softwares and codes used in this study are listed in the key resources table.
- Any additional information required to reanalyze the data reported in this paper is available from the lead contact upon request.

EXPERIMENTAL MODEL AND STUDY PARTICIPANT DETAILS

Ancient samples

We analyzed samples excavated at the Grotte Mandrin, Malataverne, France (Figure 1, Supplementary Data). The teeth and jaw fragments of Thorin, a hominin individual, were subjected to X-ray microtomographic scanning (Figure 2). One tooth root from this individual was used for genomic analyses. Thirty-three potential hominin bone fragments, in direct contact with Thorin, were subjected to ZooMS. Three of them were further subjected to Accelerator Mass Spectrometry (AMS) dating. Two complete faunal teeth (a small bison premolar and a caprinid molar) and one fragment of a Thorin tooth were submitted for U-series dating. A fossil *Hippopotamus* tooth with known isotopic ratios was used for Uranium series direct dating calibration. For carbonate isotopic analysis, tooth enamel from 5 bison, 6 red deer, 3 reindeer, 4 horses, as well as from two Neolithic humans and from Thorin were analyzed. A subsample of Thorin tooth dentine was used for collagen extraction.

These samples are listed in the key resources table and in the methods details section.

METHOD DETAILS

X-Ray microtomographic scanning of the teeth

The teeth and jaw fragments of Thorin were scanned using the X-ray microfocus instruments (X-μCT) Phoenix Nanotom 180 (FERMAT Federation from the Inter-university Material Research and Engineering Center, UMR 5085 CNRS, University of Toulouse) and GE v|tome|x s (Placamat platform, UMS 3626 CNRS, University of Bordeaux). Acquisitions were performed according to the following parameters: 100–130 kV, 170–250 μA, 1440–2550 images taken over 360° (0.14°–0.25° of angular step), 0.1 Cu filter. The final volumes were reconstructed with a voxel size of 19.5–26.3 μm for the isolated teeth and 48.1–50.0 μm for the jaw fragments.

ZooMS collagen fingerprinting

ZooMS collagen fingerprinting was carried out on 30 spatially-plotted bone fragments discovered in contact with Thorin and considered as potential hominin by basic characteristics of bone size, thickness, etc. Following ref. 42, this involved removal of collagen through decalcification with 0.6 M hydrochloric acid (HCl) overnight, ultrafiltration into 50 mM ammonium bicarbonate using 10 kDa molecular weight cut-off filters, and digestion with sequencing grade trypsin at 37°C overnight. The digests were then acidified to 0.1% trifluoroacetic acid (TFA) and then ziptipped (Varian OMIX C18 pipette tips) for peptide purification, being eluted in 50% acetonitrile (ACN) in 0.1% TFA and dried to completion by centrifugal evaporation. Samples were then rehydrated with 10 μL 0.1% TFA and 1 μL co-crystallized with an equal amount of 10 mg/mL alpha-cyano hydroxycinnamic acid in 50% ACN/0.1% TFA and allowed to dry. Peptide mass fingerprints were then acquired using a Bruker Ultraflex II Matrix Assisted Laser Desorption Ionisation Time of Flight Mass Spectrometer over the range *m/z* 700-3,700 and compared with reference spectra for humans.[41,85] The acid-insoluble pellets from specimens identified as hominin were then further processed for radiocarbon dating.

Paleoproteomic analyses

The aims of part of this study were to investigate the limitations of paleoproteomics for the diagnostic of hominin remains, in particular the extent to which proteomic approaches could generate misleading information. Semi-tryptic searches of the proteomes from Holocene AMH as well as presumed Middle Paleolithic Neanderthal remains were carried out to evaluate the error rate in identification.

Proteomes were recovered from the Holocene human specimens in three fractions per sample. All were treated with 0.6 M hydrochloric acid overnight (∼18 h), centrifuged at 12,400 rpm, and half of the supernatant ultrafiltered (10 kDa) into 50 mM ammonium bicarbonate (ABC) prior to reduction, alkylation and digestion (SOL fraction). The other half was precipitated in acetone at −20°C overnight, centrifuged and resuspended in ABC for digestion as above (PREC). Then the acid-insoluble residue was incubated with 6 M guanidine hydrochloride (GuHCl) overnight prior to being ultrafiltered into ABC as above. In each case, reduction was carried out with 100 mM dithiothreitol (DTT) in 50 mM ABC (4.2 μL in 100 μL sample) at 60°C for 10 min, allowed to cool, and acetylated with 100 mM iodoacetamide (8.4 μL in 100 μL sample) in the dark at room temperature for 45 min. The samples were further quenched with the same amount of DTT prior to digestion with 2 μg sequencing grade trypsin (Promega, UK) overnight (∼18 h) at 3°C. Sample digests (including one blank including filtered HCl, GuHCl and ABC) were then purified with C18 Solid Phase Extraction clean-up and dried to completion in a centrifugal evaporator prior to resuspension with 5% ACN +0.1% formic acid (FA) and then analyzed using LC-MS/MS (Waters nanoAcquity UPLC system coupled to a Thermo Scientific Orbitrap Elite MS) at the Biological Mass Spectrometry Core Research Facility (University of Manchester) similar to methods described in ref. 60. In brief, samples were concentrated on a 20 mm × 180 μm pre-column prior to being separated on a 1.7 μM Waters nanoAcquity Ethylene Bridged Hybrid (BEH) C18 analytical column of (75 mm × 250 μm i.d.) and fractionation was achieved using a gradient beginning at 99% buffer A/1% buffer B and finishing at 75% buffer A/25% buffer B, whereby buffer A = 0.1% FA in H_2O and buffer B = 0.1% FA in ACN. For this study, resulting MS/MS datafiles (.mgf) were searched against a local database made from the published sequences from ref. 38 and 61 using MASCOT v2.5.1. Datafiles were searched with semi-trypsin as the selected enzyme and using the following criteria: up to two missed cleavages, peptide tolerance of ±5 ppm, MS/MS fragment ion mass value tolerance of 0.5 Da, a fixed carbamidomethyl modification of cysteine (mass shift = +57.02 Da), variable deamidation of asparagine (N) and glutamine (Q) modifications (mass shift = +0.98 Da; to allow for common diagenetic alterations), and variable oxidation of methionine (M), and hydroxylation of proline (P) and lysine (K) modifications (mass shift = +15.99 Da; equivalent mass to the process of hydroxylation). Raw data can be found at FigShare: https://doi.org/10.6084/m9.figshare.16676839.

For at least two of the three anatomically modern humans analyzed, two of the three fractions gave a higher scoring protein match to the archaic COLX sequence using semi-tryptic searches than to the expected AMH sequence. The Thorin Neanderthal specimens also gave mixed results. Although the example spectrum did not yield a complete b or y ion series, those that were present around the amino acid substitution site (reflecting from both ends of the peptide) could readily be used to infer an archaic peptide despite knowing AMH as the source without setting in place standard criteria for confident semi-tryptic peptide matches. By contrast to archaeological samples, the blank run produced an order of magnitude fewer peptide matches (e.g., ∼4,000 vs. > 40,000) and Mascot scores typically of ∼5–10, whereas ∼20–100 was typically observed for our ancient samples.

Sample dating

Radiocarbon dating

Three samples from the Thorin specimen were AMS dated at the Oxford Radiocarbon Accelerator Unit (ORAU) at the University of Oxford. Collagen was initially extracted using the 'AG' protocol, comprising a simple demineralisation and gelatinisation. Following this the collagen was treated using the method outlined in ref. 44. This comprised an initial acid hydrolysis in 6M HCl. Underivatized amino acid solutions were dried down and then resuspended in 0.1 M NaOH. Following this they were separated using a Varian prep-Liquid Chromatography system. The hydroxyproline was collected in MilliQ water, then concentrated and dried using a Genevac EZ-2 Plus vacuum evaporator. Following this the samples were combusted via a PDZ-Europa Robo-Prep combustion elemental analyzer coupled to a PDZ-Europa 20/20 mass spectrometer (Sercon) operating in continuous flow mode using He gas as a carrier. C/N atomic ratios as well as $\delta^{15}N$ and $\delta^{13}C$ values, % carbon and nitrogen values, were obtained (Table S1). Following combustion the samples were graphitised and reacted with an iron catalyst in an excess of H_2 at 560°C.[86] The graphite was then AMS dated. Measurements were background corrected for the presence of trace carbon on the HPLC.[44]

Uranium series direct dating of teeth

The sample set consisted of a small bison premolar and a fragmented Neanderthal tooth (half upper crown of a molar or premolar) from the Thorin specimen, both associated with Level B2, and a caprinid molar (1996-E0-B#65) from Level B3. Teeth were sectioned in half using a high precision slow speed rotary diamond saw, exposing dentine and enamel tissues. The exposed surface of each sample was then polished to 5 microns smoothness to offer a clean ablation surface.

Uranium-series dating of the teeth was undertaken by laser ablation multi-collector ICP-MS at the Biomics Laboratory of the Geo-archaeology and Archaeometry Research Group (GARG) facility, Southern Cross University. Laser ablation was performed with a New Wave Research 213 nm laser, equipped with a TV2 cell. Thorium (^{230}Th, ^{232}Th) and uranium (^{234}U, ^{235}U, ^{238}U) isotopes were measured on a Thermo Neptune XT multi-collector ICP-MS mounted with jet sample and x-skimmer cones. All five isotopes were collected in static mode, with both ^{234}U and ^{230}Th collected in the ion counter and CDD, respectively. Helium flow rate and ICP-MS parameters were tuned with NIST610 element standard to derive a $^{232}Th/^{238}U$ ratio for this standard greater than 0.85 and thus minimize differences in fractionation between Th and U. For tuning, a fluence of 13.1 J/cm^2, pulse rate of 20 Hz, spot size of 110 μm and scan speed of 5 μm/s were used. This yielded 1.75V of ^{238}U and 1.50V of ^{232}Th on NIST610.

Teeth were ablated using rasters of 4min 54s each (two passes of ~750 μm long). Before and after each sample, NIST612, MK10 and MK16[86] standards were measured, as well as a fossil *Hippopotamus* tooth (#SCU-14033-KR) with known isotopic ratios. $^{234}U/^{238}U$ and $^{230}Th/^{238}U$ isotopic ratios were corrected for elemental fractionation and Faraday cup/SEM yield by comparison with MK10 coral for which ratios were previously characterized internally by solution analysis. Concentrations of U and Th were determined using NIST612 glass as a calibration standard. Background subtraction, concentration quantification and ratio corrections were performed using Iolite software.[62] The corrected ($^{234}U/^{238}U$) and ($^{230}Th/^{238}U$) isotope ratios for the secondary standard (MK16 coral; 1.110 ± 0.01 and 0.809 ± 0.042, respectively) were within error of the values determined by solution analysis (1.110 ± 0.002 and 0.764 ± 0.007). The calculated closed-system ^{230}Th-U age for MK16 was 120 ± 5.2 ka (2σ, n = 8), within error of the value determined by solution analysis (124 ± 2 ka). The hippopotamus tooth was used as a control on matrix effect.

Analyses of the caprinid, bison and Thorin specimens consisted of 8, 14 and 20 rasters respectively, each two passes of 750 μm long. Each raster was averaged to obtain one isotopic and age data point.

The caprinid tooth did not offer any exploitable results (thorium concentration was under detection limit) and therefore ages were not calculated. Both the bison tooth and Thorin tooth exhibited similar isotopic values, consistent with identical stratigraphic provenance and similar burying condition (Table S2). Parts of the Neanderthal tooth fragment showed some significant ^{232}Th incorporation, as well as some leaching toward the edge close to the fractured dentine, consistent with high migration of detritic thorium. Both samples showed rather heterogeneous distribution of U-series isotopes, with clusters of accumulation toward natural cracks and the enamel dentine junction. Both uranium and thorium concentrations were low, with several areas of the tooth at detection limits, leading to a relatively large uncertainty associated with the measurements. Despite a complex isotopic distribution, the diffusion pattern remained typical of what is usually observed in dental tissues. The U-series age of 43.5 ± 4.1 ka (2-sigma) for Thorin corresponding to the time at which the uranium migrated into the dental tissues, this age was considered a minimum age for the sample.

US-ESR direct dating

Two complete faunal teeth (a small bison premolar associated with Level B2, and a caprinid molar 1996-E0-B#65 from Level B3), one fragment of a *Homo neanderthalensis* tooth (Level B2) and one sediment sample (OSL sample X6717, Level B2) were submitted for U-series dating. The teeth showed very little signs of diagenetic alteration with superficial discoloration of the outer enamel and a small amount of sediment insertion in natural cracks.

An enamel fragment from each tooth was separated using a hand-held diamond saw following the protocol developed in ref. 64 and stripped of the outer ~100 microns ±10% on each side. Fragments were mounted into a parafilm mold within a Teflon sample holder to record the angular dependency in the ESR response.[87–89] Fragments were then measured at room temperature on a Freiberg MS5000 ESR X-band spectrometer at a 0.1mT modulation amplitude, 10 scans, 2mW power, 100G sweep, and 100KHz modulation frequency for ESR dating. Irradiation was performed with the Freiberg X-ray irradiation chamber, which contains a Varex VF50 X-ray gun at a voltage of 40KV and 0.5mA current on the fragment exposed to X-rays without shielding (apart from a 200um Al foil layer[90]). Each fragment was irradiated, following exponentially increasing irradiation times (around 90s, 380s, 900s, 1800s, 3600s, 7200s, 14400s, 25000s and 50000s, although the exact irradiation time and dose rate varied for each sample). For each irradiation

step, the energy output of the X-ray gun is recorded at the beginning and end and averaged, which allows correction for the dose rate received by the sample. For each irradiation step the fragment was measured over 180° in x, y and z-configurations with a 20° step.[91,63] ESR intensities were extracted from T1-B2 peak-to-peak amplitudes on the merged ESR signal. Isotropic and baseline corrections were applied uniformly across the measured spectra.[91] The amount of NOCORs was estimated using the protocol described in ref. 66, yet no influence was observed on the spectra after X-ray irradiation steps. The ESR dose-response curves were obtained by using merged ESR intensities and associated standard deviations from the repeated measurements over one orientation only. Fitting procedures were carried out with the MCDOSE 2.0 software using a Markov Chain Monte Carlo (MCMC) approach based on the Metropolis-Hastings algorithm.[63] D_E values were obtained by fitting a single saturating exponential (SSE) at the appropriate maximum irradiation dose (D_{max}), following the recommendations of ref. 71. The dose equivalent of the Neanderthal Thorin and fauna Bison teeth from B2 was estimated to be 64.1 ± 4.5 Gy and 67.0 ± 5.6 Gy respectively. Using this D_E and the parameters shown in Table S3, the US-ESR ages were unable to be modeled, likely because of U leaching and making the ESR ages younger or equivalent to the U-series ages. Thus, the equivalent dose for each sample was offset, as follows: 66.3 + 2.3/-6.7 Gy for Thorin and 68.8 + 3.8/-7.4 Gy for the Bison tooth to allow realistic modeling and creating asymmetrical uncertainties.

The age obtained for Thorin was 48 + 5/-13 ka and 49 + 5/-10 ka for the Bison tooth. When assuming a closed system model, Thorin's age estimation became 56 ± 41 ka and the Bison fauna age became 56 ± 39 ka, corresponding to maximum ages for these fossils. A simple early uptake model gave an age estimation of 42 ± 5 ka for the fauna. The US-ESR ages of Thorin and the bison tooth was modeled by considering dosimetry from the C2 layer or a mix B2/C2 values. Using the parameters from C2 or average C2/B2, Thorin age estimates were slightly shifted to 51 + 4/-14 ka and 50 + 5/-13 ka, and the bison tooth to 51 + 4/-10 ka and 50 + 5/-10 ka, respectively. Therefore, all age estimates were statistically indistinguishable regardless of the stratigraphic association with B2, C2 or an average B2/C2. For the Bayesian model, all systematic errors were removed and all associated uncertainties defined at 1-sigma. This resulted in a US-ESR age estimate of 48 ± 4 ka for Thorin, which was included as the likelihood in the OxCal model.

The external beta dose rates for the sediment sample have been calculated from the U, Th and K contents measured on a portion of OSL sediment X6717 from B2[1] sub-sample (~8 g) by ICP-MS and ICP-AES (Table S3). The external gamma dose rates were determined from carbon-doped aluminum oxide dosimeters buried in close proximity to the location of the sediment sample for a period of 396 days. The cosmic dose rate has been calculated for the specific burial depth of the fossils according to ref. 72, taking into account the altitude, geomagnetic latitude, density of sediment overburden, and the time-averaged geometry of bedrock overburden.

Bayesian model for Thorin age

We built a simple Bayesian model using OxCal 4.4.3[64] and the INTCAL20 calibration curve[92] to determine a modeled age for Thorin. Thorin is linked stratigraphically with the PN2 (Post-Neronian 2) levels of the site, encompassing levels C2 to B2. For this reason we used the dated boundaries from the Bayesian model derived in ref. 1 as cross-referenced constraints on the age in a single Phase model aimed at providing a probabilistic density function for the age of the Thorin remains. For Thorin's age estimate we used an error-weighted mean of the three HYP radiocarbon ages in fraction modern of 0.0007 ± 0.0007 fM (T = 2.64, $\chi 2$ = 5.99, df. = 2), as well as the U Series and ESR age estimates constrained as minimum and direct ages respectively. Outliers were set at 0.05 probability within a General Outlier_Model.[93] All posterior outliers were set at <5%. The CQL code for this is below.

The results of the modeling are shown in Figure 4. We used a Date command embedded with the phase to determine an age range for Thorin at 51,300-48,900 cal. BP (at 68.2% prob. and 52,900-48,050 cal. BP (95.4% prob.)).

The Bayesian Model CQL code for Thorin age is as follows:

```
Sequence()
{
Boundary(" = Start C2 Post Neronian");
Phase("Thorin phase")
{
Combine("Thorin")
{
Before()
{
Date("Thorin USeries",N(2021–43500,2050))
{
Outlier("General", 0.05);
};
};
R_F14C("HYP dates", 0.0007, 0.0007)
{
Outlier("General", 0.05);
};
Date("Thorin ESR",N(2021–48000,4000))
{
Outlier("General", 0.05);
```

};
Date("Thorin date est");
};
};
Boundary(" = End Post-Neronian 2/Start Sterile");
}.

Isotopic analyses (C, O, Sr)

The goal of performing stable isotopic analyses of tooth enamel (carbon $\delta^{13}C$, oxygen $\delta^{18}O$, strontium $^{87}Sr/^{86}Sr$) and bone or dentine collagen (carbon $\delta^{13}C$, nitrogen $\delta^{15}N$) was to gain information on the paleoenvironmental context of Thorin, its position in the large mammal trophic system and its mobility pattern. These newly obtained data could be compared with those obtained for faunal remains from sites in the same region and for other late Neanderthal specimens in western Europe. Since carbon, nitrogen and oxygen isotopic ratios depend on the type of vegetation at the basis of the food webs (open or forested), aridity, plant productivity, temperature, geological bedrock, and, for humans, on the trophic position and the prey selection,[94,95] this multi-isotopic approach allows us to refine the palaeoenvironmental context of this Neanderthal and to confirm its chronological attribution. For this study, fossil tooth material from faunal and human specimen from Grotte Mandrin were analyzed (see below) and published data for the sites of Payre in the same region were used for comparison of carbon, oxygen and strontium isotopic values of tooth enamel,[96–98] while sites such as Aldène Cave, Mialet Cave, Abri du Maras, Trou de la Mère Clochette, Saint-Marcel Cave were used for comparison of carbon and nitrogen isotopic values of bone collagen[99–103] as well as previously published data on identified fauna from Grotte Mandrin[4] were used for comparison of the carbon and nitrogen isotopic values of bone and tooth collagen.

Carbonate isotopic analysis

For carbonate isotopic analysis, tooth enamel was sampled from animal teeth from levels B and C in Grotte Mandrin, for the following large mammal taxa: bison *Bison priscus* ($n = 5$), red deer *Cervus elaphus* ($n = 6$), reindeer *Rangifer tarandus* ($n = 3$) and horse *Equus cf. germanicus* ($n = 4$). In addition, one tooth enamel fragment from Thorin was analyzed, as well as two modern human teeth from Neolithic context in the same cave as comparison.

For the newly analyzed specimens, about 5–10 mg of tooth enamel were drilled using a rotating tool with diamond coated drill bit and the powder was then pretreated following the protocol from ref. 86 to remove possible organic and carbonated contamination. Subsequently, the C and O isotopic analysis was performed at the Department of Geosciences of the University of Tübingen as follows: pretreated enamel was reacted with 100% H_3PO_4 for 4 h at 70°C using a MultiFlow-Geo interfaced with an Elementar IsoPrime 100 IRMS. Final isotopic ratios are reported as delta values per mil (‰) relative to an international standard (V-PDB for carbon and oxygen), calibrated with international standards (IAEA-603: $\delta^{13}C = +2.46‰/\delta^{18}O = -2.37‰$ and NBS-18: $\delta^{13}C = -5.014‰/\delta^{18}O$: $-23.2‰$), as well as three in-house standards. Multi-point standard isotope calibration was carried out using the IonOS software (Version 3.2) by Elementar by generating a trend line (y = mx+c) that maps measured vs. expected isotopic results, which is then used to calibrate sample results.

The measurement uncertainty was monitored using three in-house standards. The overall analytical precision is higher than 0.1‰ for $\delta^{13}C$ values and better than 0.2‰ for $\delta^{18}O$ values. The conversion of $\delta^{18}O$ values toward the V-SMOW standard has been done using the formula: $\delta^{18}O_{V\text{-}SMOW} = \delta^{18}O_{V\text{-}PDB}.1.03096–30.86$.

The $\delta^{13}C$ values of Thorin were about 3‰–4‰ lower than those of the coeval ungulates and in the same range as those of Neanderthals from Payre.[97] Such a difference is typically found for Pleistocene hominins in Europe.[97,104] Since the $\delta^{18}O$ values of Thorin were similar to those of coeval fauna, and much lower than those of Holocene humans living under interglacial conditions from Mandrin and Payre, the combined $\delta^{13}C$ and $\delta^{18}O$ values of this hominin were fully consistent with a life in the same environmental conditions as the ungulates from the MIS3 layers where it was found.

The strontium isotopic analysis was performed on pretreated enamel powders at the clean laboratory facilities of the Curt-Engelhorn Center for Archaeometry at Mannheim, Germany, following a well-established protocol.[105] The determination of $^{87}Sr/^{86}Sr$ ratios was performed by a high-resolution multi collector ICP-MS (HR-MC-ICP MS, Neptune). Raw data were corrected according to the exponential mass fractionation law to $^{88}Sr/^{86}Sr = 8.375209$. Blank values were lower than 50 pg Sr, corresponding to less than 0.1% of the Sr-content of the analyzed sample.

When compared to the range of variation for $^{87}Sr/^{86}Sr$ ratios in Southeastern France, as reported in Figure 7 of ref. 79, $^{87}Sr/^{86}Sr$ ratios measured here (Figure S3) were broadly spread. It was therefore not possible to establish an exact location of the Mandrin Neanderthal at the time of its tooth formation, but nothing indicated that this individual would have spent some of this youth far away from the location of Grotte Mandrin.

Collagen isotopic analysis

A very small fragment (~100 mg) of Neanderthal tooth dentine was treated following a well-established protocol[106] at the University of Tübingen. The sample was ultrasonicated in acetone and then rinsed with distilled water. Once dried, it was powdered and sieved to a particle size of less than 0.7 mm. For collagen extraction, bone powder was decalcified in 1 M HCl for 20 min at room temperature and filtered through a 5 mm filter. The insoluble residue was then soaked in 0.125 M NaOH for 20 h at room temperature. Subsequently, the rinsed residue was heated in closed tubes at 100°C for 17 h in HCl pH2 solution, in order to gelatinize the collagen. After filtration through a 5 mm filter, the filtrate containing gelatinized collagen was freeze-dried.

The stable carbon and nitrogen isotopic compositions were performed in duplicate at the Institute of Environmental Science and Technology (ICTA, Barcelona, Spain) using a Thermo Flash 1112 (Thermo Scientific VC) elemental analyzer coupled to a Thermo Delta V Advantage mass spectrometer with a Conflo III interface. This measures the ratios of $^{13}C/^{12}C$ and $^{15}N/^{14}N$ relative to an international standard (V-PDB for carbon and AIR for nitrogen). The international laboratory standard, IAEA 600 (caffeine), was used. Analytical uncertainty was determined to be $\pm 0.20‰$ for both $\delta^{13}C$ and $\delta^{15}N$, based on multiple measurements of collagen extracted from modern bones of camel (*Camelus dromedarius*) and elk (*Alces alces*). The resulting values (fC/N ratio of 3.4 and carbon and nitrogen content of 34.7% and 12.0%, respectively) were in the range of well-preserved collagen.[107,108] The $\delta^{13}C$ and $\delta^{15}N$ values of $-19.5‰$ and $+11.7‰$, respectively, were within the range of those obtained for other Middle and Late Pleistocene hominins.[104,109–111]

The analyzed Thorin specimen was a tooth while the other specimens, including published data, were bones, leading potentially to slightly higher $\delta^{15}N$ values. A change of baseline has also been documented in France around the time of Thorin.[111] To investigate these interferring factors, we gathered isotopic data from other sites in the same region (Southeastern France) at around the same time, and compared these values to those of Southwestern France around the Neanderthal site of Saint-Césaire (Figure S3). Despite slightly lower $\delta^{15}N$ values in Southeastern France compared to those of Southwestern France, the isotopic values of Thorin were plotting in the same position compared to the herbivorous species as in Saint-Césaire, indicating that Thorin had a similar trophic position in its ecosystem as the late Neanderthal from Saint-Césaire. There was no indication that the Neanderthal from Grotte Mandrin could not be part of the ecosystem represented by the faunal remains in the region.

Sample processing for DNA sequencing

The different DNA sample preparation steps and sequencing run types performed for each sequencing library are summarized in Table S4.

DNA extractions

Sample processing was performed in a dedicated clean laboratory facility at the Lundbeck Foundation Center for GeoGenetics, GLOBE Institute, University of Copenhagen, Denmark, following strict ancient DNA procedures. Each extraction, and subsequent USER treatment, library building, and PCR setup session included a mock reaction where no sample (for extraction) or QIAGEN© EB buffer (for the following steps) was added to the reagents instead of DNA solution. These pre-PCR steps were performed in the ancient DNA facility, physically separated from laboratories where post-PCR and fresh modern samples are processed.

The surface of a first molar root (sample MAN-15-B2-1600, also registered under the GeoGenetics accession number CGG_2_016357) was cleaned by gentle abrasion, and 280mg of the root tip was manually crushed using a mortar. DNA was extracted following a silica-column based method described in ref. 95 and adapted by ref. 96 (method Y). Root fragments were predigested for 2h at 37°C by incubating in 1mL of an extraction buffer (0.45M EDTA, 0.25 mg/mL Proteinase K and 0.5% N-LaurylSarcosyl). After centrifugation for 2 min at 13,000 rpm, the supernatant was removed and the remaining pellet was subjected to three sequential digestions as described below.

After 24h of incubation at 37°C in fresh digestion buffer, the microtube was centrifugated for 2 min at 13,000 rpm and the supernatant E1 (labeled as BE1 for the extraction blank) was recovered without disturbing the remaining undigested pellet. This pellet was further incubated with 1mL of fresh digestion buffer for an additional 42 h at 37°C, centrifugated for 2 min at 13,000 rpm and the supernatant E2 (BE2 for the extraction blank) was recovered. As there was still undigested material, a final incubation of 72 h at 37°C in fresh digestion buffer was performed, and supernatant E3 (the extraction blank being labeled as BE3) recovered after centrifugation for 2 min at 13,000 rpm. For any incubation lasting for more than 24h, 0.25 mg/mL of fresh Proteinase K was added after each 24 h of incubation.

Each of the supernatants E1, BE1, E2, BE2, E3 and BE3 was concentrated down to 200μL volume using an Amicon Ultra-4 30kD device (Merck Millipore). DNA solutions were further purified on a MinElute column (QIAGEN©) and eluted in 60μL elution buffer (QIAGEN© EB supplemented with 0.05% Tween 20) after 15 min incubation at 37°C. All extracts were stored at −20°C in siliconized tubes (Eppendorf LoBind).

USER treatment, sequencing library building, and indexing

A fraction of 14.9μL of each extract was directly built into Illumina sequencing libraries to validate the presence of postmortem DNA damage signatures. Another fraction (32.5μL) of each extract was incubated for 3h at 37°C with 10μL Uracil-Specific Excision Reagent (USER, NEB reference M5505) enzyme mix in order to remove uracil residues and limit the impact of nucleotide mis-incorporations in the analysis.[112]

On each extract, multiple independent library constructions and amplifications aim at limiting PCR duplicates and thus reducing sequencing costs (Table S4). Blunt-End Illumina sequencing libraries were built on both USER-treated and non-USER-treated extracts, following ref. 98 with slight modifications as described in ref. 99, using the NEBNext DNA Library Prep Master Mix Set (NEB reference E6070) without the ssDNA isolation module.

To determine the optimal number of Polymerase Chain Reaction (PCR) cycles to be used for amplifying libraries, an aliquot of 1μL of each library was diluted 20 times and subjected to a real-time PCR assay, as recommended in ref. 97. Subsequently, a volume of 12μL (out of the 25μL total library volume) of each unpurified library was amplified in a PCR reaction volume of 50μL, using the KAPA HiFi HotStart Uracil+ ReadyMix (KAPA Biosystems, Inc), 200nM of PCR primer IS4[112] and 200nM of a custom-designed primer containing a 6-bp known index sequence used for post-sequencing demultiplexing. Thermocycling conditions were as follows: 1 min at 94°C, followed by N cycles of 15 s at 94°C, 20 s at 60°C, and 20 s at 72°C, and a final elongation step of 1 min at 72°C. The cycle

numbers N used for each library amplification are summarized in Table S4. When less than 12 cycles were necessary, libraries were subjected to a single PCR amplification round, purified on a MinElute column (QIAGEN©) and eluted in 20 μL EB with 0.05% Tween.

Otherwise, PCR amplification was carried out in two rounds: after the first 10–12 cycles amplification round, PCR products were purified on a MinElute column, eluted in 20 μL EB (QIAGEN©) and split over four PCR reactions. The four final PCR products were then pooled and purified on a MinElute column and eluted in 10 μL EB with 0.05% Tween. A 1/10 dilution of each purified product was quantified on an Agilent 2200 TapeStation instrument (Agilent Technologies).

Whole Genome Enrichment

To increase the human DNA fraction in the sequencing libraries, we performed an in-solution Whole Genome Enrichment (WGE), using MYBaits RNA probes synthesized at MYcroarray (Ann Arbor, MI, USA[113]). Following manufacturer's instructions (MYbaits manual v2.2), 70 to 650ng of amplified libraries were incubated for 40 h at 55°C with 5μL of the synthetic probes (one capture reaction per library), in presence of blockers (Human Cot-1 DNA, Salmon Sperm DNA and Proprietary Blocking Agent). After purification using Dynabeads MyOne Streptavidin C1 beads (Invitrogen), captured libraries were eluted in 30 μL EB with 0.05% Tween. Real-time PCR was performed on a 1/20 dilution of the eluate, to determine the minimal number of PCR cycles required to amplify the captured libraries up to a molarity compatible with the Illumina sequencing technology. The whole volume of WGE-enriched libraries was then amplified in a 100μL final PCR reaction, with 2μL of AmpliTaq Gold DNA Polymerase (Applied Biosystems) and 200nM of each primer IS5_reamp.P5 and IS6_reamp.P7,[114] for 7 to 13 cycles (Table S4). Thermocycling conditions consisted of initial denaturation for 5 min at 94°C, followed by N cycles of 30 s at 94°C, 30 s at 60°C and 40 s at 72°C, and lastly an elongation step of 7 min at 72°C. Amplification products were purified on MinElute column and eluted in 20 μL EB + 0.05% Tween.

DNA sequencing

Purified libraries were quantified on an Agilent 2200 TapeStation instrument (Agilent Technologies) and pooled, requiring at least three base differences between any indices pair. Pools were quantified using a Kapa Library Quantification Kit Illumina (KapaBiosystems, KK4854) real-time PCR assay and sequenced at the Danish National High-Throughput DNA Sequencing Center, Copenhagen University, Denmark, on an Illumina HiSeq2500 platform, with 100SR, 100PE or 80PE mode, with single i7 index read. Basecalling and demultiplexing were performed using CASAVA v.1.8.2.

DNA sequencing data analysis

Sequencing reads processing and mapping

Illumina reads were processed for each individual library using the PALEOMIX v1.1.1 pipeline[65] with default parameters, except that minimal mapping quality threshold was set to 30 and seeding was disabled. Briefly, sequencing reads were trimmed for known adapter sequences, low quality termini, and filtered out if shorter than 30 nucleotides using AdapterRemoval.[66] Paired-end reads overlapping for 11 nucleotides or more, with a maximal edit distance of 1, were collapsed and further treated as single-reads. Trimmed and collapsed reads were aligned to the human reference genome hg19 available from the UCSC genome browser (http://hgdownload.cse.ucsc.edu/goldenPath/hg19/chromosomes/) using BWA version 0.5.9-r26-dev,[67] collapsed for duplicates and re-aligned locally around indels using GATK.[68] Uncollapsed paired-end reads most likely correspond to long contaminating DNA templates of modern origin and were thus filtered out of the final BAM file.

The whole procedure was repeated against the revised Cambridge reference mitochondrial sequence (rCRS, Accession Number NC_012920)[59] to generate mitochondrial read alignments. Summary statistics obtained from PALEOMIX are presented in Table S5.

Sequencing data authentication and contamination estimation

Authentication of damaged ancient DNA fragments

Presence of ancient DNA was confirmed using mapDamage2.0[70] by detecting excess C to T substitutions in the strand termini of each generated library (Table S8, and Figure S4). The non-USER treated library from extract 1 (Thorin_1600_E1L1P2) had significantly less fragments with deamination patterns compared to the other non-USER treated libraries (Table S8).

aRchaic[71] was used to detect additional types of damage patterns by applying a grade membership model, which clusters the tested samples into groups based on their mismatch profiles. In contrast to mapDamage, *aRchaic* not only looked for signs of cytosine deaminations, but detectsed a range of non-predefined damage patterns. Therefore, BAM files from all libraries, regardless of whether they have been USER-treated or not, were relevant as input. *aRchaic* returned Mismatch Feature Format (MFF) files for each of the tested libraries containing the information of mismatch types, flanking bases, strand break bases and positions of the observed mismatches. Based on the detected features, the mismatches were clustered into groups called mismatch profiles. The number of profiles used for the analysis were defined by *K*. The grade of membership was determined by the relative frequency of each mismatch profile observed in the individual samples. The implemented model assumed each of the mismatches observed in the samples belonged to one of the *K* mismatch profiles.

All BAM files were down-sampled to 10,000,000 reads. We used data from 22 libraries of the Thorin sample along with 33 archaic individuals,[8,11,12,15,16,47,53] 10 ancient samples,[9,115–123] and 39 modern human individuals[124] for reference. The results of $K = 2$ displayed the difference in the level of cytosine deamination patterns between modern, non-USER treated ancient, and USER-treated ancient libraries (Figure S5). For $K = 4$, the modern samples were primarily assigned to cluster 1, while the libraries generated on the Neanderthal fossils presented in ref. 16 were mainly assigned to cluster 2. The non-USER treated ancient libraries were displaying a high level of membership in cluster 3 and USER-treated libraries were mainly assigned to cluster 4 (Figure S6). Thus, USER-treated

ancient libraries could be distinguished from libraries containing modern DNA, meaning that a significant membership in cluster 1 for the ancient libraries was an indication of contamination of modern DNA. Considering this, we observed that extract E1 of the Thorin sample contained relatively high amounts of modern contamination compared to extracts E2 and E3.

Estimation of sequencing error. We, furthermore, estimated the level of sequencing errors in the libraries following the approach in ref. 118. The method is based on measuring an excess amount of derived alleles relative to a high quality genome, which is assumed to be error-free, using ANGSD.[72] As our high quality sample, we used present-day Mbuti individuals from Simons Genome Diversity Panel.[124] In order to define the ancestral allele states of each polymorphism, the method required an outgroup, for which we used a chimp genome. Only the intersection of sites covered by the test sample, the error free individual and the outgroup were considered by the method (Figures S7, and S8).

Mitochondrial contamination estimates. We carried out contamination estimations based on the mtDNA using *ContaMix*[73] (Table S6). We used *BCFtools v.1.10.2* (https://github.com/samtools/bcftools)[74] to generate a consensus sequence for each library. Each of the consensus sequences were aligned to 311 present-day human mtDNA sequences with *mafft*.[75] We, additionally, mapped the BAM files to their respective consensus sequences with the *BWA* package.[67] We discarded unmapped reads, reads below mapping quality 30, and reads with alternative hits using *SAMtools*,[69] so that only uniquely mapped reads were kept for further analysis. Both the mt alignment as well as the remapped BAM file were used as input to *ContaMix*.

The resulting point estimates of the mtDNA contamination indicated that libraries built on extract E1 were significantly contaminated compared to extracts E2 and E3 (Table S6). Additionally, we ran the analysis on a merged BAM file including data from all libraries with a resulting point estimate of authentic reads at 0.77. Excluding extract E1 decreased the level of contamination significantly to a proportion authentic of 0.997.

X chromosome contamination. X chromosome contamination estimates were carried out using ANGSD by generating a binary count file covering sites on the X chromosome with a base quality of at least 20 (-r X: –doCounts 1 –iCounts 1 –minQ 20). The count file was used as input along with a HapMap file of CEU (Europeans) to the contamination estimator, from which maximum likelihood estimates of contamination levels were obtained (Table S7). Extract E1 was significantly more contaminated than extracts E2 and E3, which influenced the overall level of contamination in the merged BAM file containing the reads of all libraries. We therefore assessed the level of nuclear contamination in the BAM file including all reads excluding extract E1, from which a reduced amount of contamination at ~0.01 was obtained (Table S10). Due to the consistent observations of extract E1 being more contaminated relative to extracts E2 and E3, data from sequencing libraries built from extract E1 were excluded in all subsequent analyses.

Mitochondrial DNA (mtDNA) and Y chromosome analysis

Metagenomic classification of reads from sediment samples

Sediment samples[14] included in the mtDNA analysis were processed through the metagenomic classifier *KrakenUniq v. 0.5.8*.[76] We filtered the raw alignments (obtained from European Nucleotide Archive, accession PRJEB42656) to only include reads with at least 35 base pairs and mapping quality of at least 25 and performed metagenomic classification using a custom database of all full mitochondrial and plastid genomes in RefSeq. All reads classified within the genus of primates were used for further analysis. Variant calling was carried out with '*bcftools call*' (-m –ploidy 1) and filtered for sites with read depth of $\geq$5 and genotype quality of $\geq$25. To ensure that only confidently called sites were used for analysis we excluded sites where the genotype was supported with less than 75% of the reads. Excluded sites were set to missing in the final consensus calling generated by using '*bcftools consensus*'.

mtDNA analysis

Maximum likelihood approach

We studied the phylogenetic relationship between Thorin and previously published Neanderthals using a Maximum Likelihood (ML) approach based on the mtDNA. We included 43 ancient humans,[115,125,126] 34 Neanderthals,[8,11,12,16,33,43,45,47,127–131] and 4 Denisovans.[46,131–133] We carried out the genotype calling for Thorin using '*bcftools call*' (-m –ploidy 1) and only considered sites covered by at least 5 reads with a genotype quality of at least 30. We generated the consensus sequence with '*bcftools consensus*'. Sites not passing the filtering were set to missing in the final sequence. In order to identify possible ambiguous genotypes in the consensus sequence we computed the frequency of the alternate allele across all sites along the mitochondrial genome (Figure S9). All the sequences were aligned using *mafft*[75] and inputted to the ML tree inference tool *RAxML-NG*.[77] The tree was inferred using 100 bootstraps under the GTR-I-G4 substitution model (options: –all –bs-trees 100; Figure S10).

Maximum parsimony (MP) analysis between Neanderthal mtDNA sequences

We furthermore performed a maximum parsimony analysis using Denisova 3 and 23 Neanderthals (included in the ML analysis) only considering sites within the coding region (rCRS coordinates: 577-16,023). Using the *pratchet* function from the R package *phangorn*,[78] a distance matrix was computed including raw substitution rates, which was used to perform a branch-shortening analysis.[8] Relative age estimates were obtained using Goyet Q56-1, which has been radiocarbon dated to be 42,540 years old,[16] as a reference sample. The final age estimated were computed using the substitution rate of the coding region in modern humans, 1.57×10^{-8} substitutions/bp/year (95% confidence interval (CI): 1.17×10^{-8}-1.98×10^{-8} substitutions/bp/year[77]). The phylogeny was similar as observed in the ML analysis (Figure S10), with Thorin forming a clade with Forbes's Quarry (FQ) and Stajnia S5000. Thorin shared an additional substitution with FQ in comparison to Stajnia S5000. Thorin had a similar age as FQ and was slightly younger than Stajnia S5000 (Figure S12). However, the age estimated on FQ should be treated with caution, since only ~80% of the mt genome was

available for analysis.[47] The obtained age for Thorin (95% confidence interval: ~80–100 ka) was significantly older than the age of the stratigraphic layer from which it was excavated. A similar age discrepancy was found in the analysis of Stajnia S5000 and Chagyrskaya 8, which have both been molecularly dated to be older than what their respective radiometric contexts suggest.[15,45]

Molecular tip dating and divergence date estimates from Neanderthal mtDNAs

BEAST v. 2.6.3[49] was used to perform molecular tip dating on Thorin and to estimate divergence dates. The analysis included 24 Neanderthals,[11,16,33,126] 1 Denisovan,[134,135] 9 ancient human genomes,[125,126] and 53 contemporary human mitochondrial genomes.[136] We aligned the sequences with *mafft* and constrained our analysis to the non-D-loop region (rCRS coordinates: 577–16023 bp) in order to avoid the hypervariable regions of the genome. For the initial runs, we performed two sets of analysis, one with a fixed substitution rate of 1.57×10^{-8} substitutions/bp/year, assuming a similar mitochondrial substitution rate as for modern humans, and another with an estimated substitution rate.

Previously radiocarbon- and molecularly dated samples were used as calibration points (Table S11), where the point estimates were used as initial values and their corresponding 95 Confidence Intervals (CI) were used as a uniform prior for the respective samples. For undated Neanderthals, an initial value of 50,000 years ago along with a uniform prior ranging from 30,000 to 300,000 years ago was used. A uniform prior to the TMRCA of all Neanderthals was set to 100,000-infinity, while a uniform prior for the TMRCA of modern humans was set to 50,000-infinity.[37] We set the age of present-day humans to 0 with no prior distribution.

The optimal substitution model supporting our data was determined using the BEAST package *bModelTest*.[79] For our data the best fitting model was Tamura-Nei 1993 (TN93)[137] including rate heterogeneity and invariable sites. To determine the best fitting combination of a clock (strict clock or relaxed clock log normal) and a tree model (Coalescent Bayesian Skyline (CBS) or Coalescent Constant Population (CCP)), a marginal like estimation (MLE) analysis was performed for each model combination using stepping-stone (SS) sampling from the BEAST2 *model-selection* package with alpha set to 0.3 and a preBurnin percentage of 10%. For each clock/tree model combination, 100 steps with a chain length of 15,000,000 were run in order to ensure convergence of the majority of the steps. Following ref. 140, the models with CBS were strongly favored over CCP (fixed substitution rate: $\log_{10}$ BF > 30, estimated substitution rate: $\log_{10}$ BF > 26). No notable difference between the strict and relaxed clock log normal models (fixed substitution rate: $\log_{10}$ BF > 0.17, estimated substitution rate: $\log_{10}$ BF > 0.4) was observed, however the relaxed clock model was chosen as it is a slightly better fit and allows for varying substitution rates between branches.

Four independent MCMC runs were then performed with 75,000,000 iterations and 225,000,000 iterations for the analysis with fixed and estimated substitution rates, respectively. A burn-in of 10% was used, while sampling parameters and trees for every 10,000 iterations. The independent runs were then combined respectively using *LogCombiner* in order to generate the final maximum clade credibility tree with *TreeAnnotator*. Age and divergence date estimates are presented Figure S12 and Tables S14 and S15. The mean substitution rate was estimated to 1.76×10^{-8}.

To test if a slower rate in the "Thorin-clade" would form a plausible explanation for the discrepancies observed between the molecular and contextual ages of the Neanderthal samples in that clade, we carried out another BEAST analysis using the same sequence alignment but adding Thorin as an additional calibration point with a mean age of 50 ky (95% CI: 45–55 ky) while estimating the substitution rate. For the analysis, TN93 was used as a substitution model allowing for rate heterogeneity and invariable sites. The relaxed clock model was used in order to obtain rate estimates for each branch of the tree and combined it with the CBS tree model, which was strongly favored over CCP ($\log_{10}$ BF > 26). We ran four independent runs of each 100,000,000 iterations of which 10% was used as burn-in. Both tree and parameters were sampled for every 5,000 iterations. The runs were subsequently combined using *LogCombiner*, from which we generated the maximum clade credibility tree using *TreeAnnotator*. Age and divergence date estimates are presented Figure S12 and Tables S14 and S15. The mean substitution rate was estimated to 1.82×10^{-8} substitutions/bp/year. Phylogenetic trees obtained with BEAST are presented in Figure S13.

Y chromosome analysis

The sex determination was performed based on reads aligned to X and Y chromosomes[52] (Table S10). Phylogenetic analyses of the Thorin Y chromosome sequence were carried out using a reference panel of shotgun sequencing data for 21 human samples (19 high coverage ancient samples; 2 modern samples with A00 haplogroup) and nine archaic humans (seven Neanderthals and two Denisovans; Table S11). Individual sample genotypes on shared variant sites (minor allele count (MAC) $\geq$ 2) were obtained by selecting the majority allele at each genomic site covered by a minimum of two sequencing reads, with the further requirement that >80% of reads show the majority allele. Singleton (MAC = 1) transitions were kept if covered by at least four sequencing reads, while singleton transversions were included if covered by at least three reads. The final set of variant sites were obtained by filtering for biallelic SNPs across all samples and restricting to the ~6.9 Mb long "accessible" Y chromosome regions targeted by the capture probes in ref. 141. For analyses including the lower coverage El Sidrón 1253 sample, we merged sequencing reads obtained from the reduced ~560 kb capture region with reads obtained from the exome region captured in that individual. The phylogenetic tree was reconstructed using RaxML-NG under the substitution model GTR+G+ASC_LEWIS using 300 bootstraps (options: –all –bs-trees 300) with the alleles observed in the Chimpanzee genome as outgroup on a final set of 6,717 SNPs.

Population genetic analyses

Analysis panel

A panel of 30 contemporary individuals,[124] 18 high quality ancient genomes,[9,115–122,138] and 14 archaic genomes[8,11–13,15,16,45,47,53,123] was used (Table S9). Radiocarbon dates used for calibration are indicated in Table S13. Low coverage Neanderthals were filtered with

SAMtools v. 1.3.1[69] to discard reads with a mapping quality below 25. We kept two versions of each low coverage sample, one BAM file including all reads, while the second only contained deaminated reads. Both sets were obtained using pseudo haploid genotyping by sampling a random allele on each site.

We carried out a two-step approach to combine the data of the high and low coverage Neanderthals. We first selected all biallelic SNPs from previously published diploid genotype calls for the four high-coverage Neanderthals, and extracted pseudo-haploid genotypes from the low coverage data subset at the same sites. Genotypes in the low-coverage samples that did not match either of the two alleles observed in the high-coverage samples were set to missing. We then extracted biallelic SNPs segregation among the low-coverage samples only, and merged both sets. For the final analysis panel, we including only biallelic transversion SNPs, as well as restricting to regions within the 1000 Genomes Phase 3 strict accessible genome mask (ftp://ftp.1000genomes.ebi.ac.uk/vol1/ftp/release/20130502/supporting/accessible_genome_ mask s/20141020.strict_mask.whole_genome.bed) ending up with 15,312,074 SNPs in the full dataset.

Procrustes analysis

We used procrustes analysis[139] to place the low-coverage Neanderthals within the context of a principal component analysis (PCA) of the three high coverage samples Altai Neanderthal, Vindija 33.19, and Denisova 3. The data was filtered with PLINK v. 1.9[80] to keep sites with minor allele frequencies above 0.05 and no missing genotypes. Procrustes analysis was then carried out by first performing a PCA with EIGENSOFT[81] using the Altai Neanderthal, Vindija 33.19, and Denisova 3. Subsequently, we obtained raw PC coordinates for each low-coverage Neanderthal sample by individually projecting them onto the three reference samples. The obtained raw PC coordinates were then transformed to align with the reference PCA coordinates by using the *procrustes* function from the R package *vegan*[82] (Figure S14).

D-statistics

In order to assess the relationship between the archaic individuals, different configurations of D-statistics were carried out using ADMIXTOOLS 2.0 (https://uqrmaie1.github.io/admixtools/)[140] in R (Tables S17, S18). All estimates were obtained using a block jackknife with a block size of 5 centiMorgan. We first tested for differences in levels of allele sharing between Neanderthals and present-day human populations by using *D* (Vindija 33.19/Altai Neanderthal, low; modern, Mbuti), where 'low' represents all the low coverage Neanderthals including Thorin, while 'modern' represents a number of contemporary and ancient individuals. We carried out all D-tests by using either all fragments or restricting to only deaminated reads in the low coverage Neanderthal samples (Figures S15, and S16).

A similar test with the configuration *D (Thorin, Neanderthal X; Human reference genome, Mbuti)* was carried out to test for reference bias in Thorin compared to other low coverage Neanderthals (Figure S17). Likewise we tested for potential capture bias in our data with the D test *D(capture, shotgun; reference, Mbuti)*, testing our capture reads used throughout this study and a set of reads generated without capture for significant allele sharing with the reference genome (Figure S17). The D-test *D (Thorin, Neanderthal X; Han/French, Mbuti)* was carried out to further investigate the possibility of additional allele sharing between Thorin and modern humans (represented by Han and French populations) compared to the other low coverage Neanderthals (Figure S17).

The relative amount of allele sharing of Thorin and other Neanderthals with the two high coverage samples Vindija 33.19 and Altai Neanderthal was next authentified using D-statistics of the form *D* (Altai Neanderthal, Vindija 33.19; Neanderthal X, Mbuti; Figures 5 and S19). Using D-statistics of the form *D* (Vindija 33.19, Thorin; Neanderthal X, Mbuti; Figures 5 and S19), and *D* (Vindija 33.19, Neanderthal X; Thorin, Mbuti; Figure S20), we explored if Thorin is consistent with forming an outgroup with respect to other Neanderthal samples after 80 ka, including the ~70 ka Mezmaiskaya 1 individual from the Caucasus as well as the ~80 ka Chagyrskaya 8 individual from Siberia.

Finally, we tested for signature of gene flow from a "deep" lineage into late European Neanderthals using D-statistics of the form D (Vindija 33.19, Neanderthal X; Mezmaiskaya 2, Mbuti), D (Mezmaiskaya 2, Neanderthal X; Vindija 33.19, Mbuti), and D (Vindija 33.19, Mezmaiskaya 2; Neanderthal X, Mbuti; Figure S20).

Treemix

To infer a tree topology using the allele frequencies from 354,021 SNP sites, treemix analysis[83] was carried out. Due to the differences in the level of contamination, analysis were restricted to deaminated fragments from samples with significant signs of modern contamination (Mezmaiskaya 1 and 2), while all obtained reads passing the initial filtering steps were used for Thorin, Goyet Q56-1, and Les Cottés Z4-1514 (Table S16). Two high coverage Mbuti individuals from Simons Genome Diversity Panel[124] (sample IDs: HGDP00456, SS6004471) were used as a root population. The analysis was carried out grouping SNPs into blocks of 300 bp (-k 300) to account for linkage disequilibrium without the default sample size correction (-noss).

The model with no migration event, placing Thorin as an outgroup to the rest of the late European Neanderthals as well as Mezmaiskaya 1 is presented Figure S21. The relatively high residual values between some of the Neanderthals indicated that the initial model fails to fully resolve the relationships between the tested samples. Another treemix analysis allowing for one or two migrations event was therefore carried out (Figure S21).

Runs of homozygosity

Runs of homozygosity (ROH) were called by employing spatial smoothing by fused lasso regression of read allele frequencies along individual Neanderthal genomes. In this approach, the vector of minor read allele frequencies was used as a predictor variable in a regression that aims to estimate a piecewise constant vector of coefficients by penalizing differences in consecutive coefficients. The goal of this approach was to find long stretches with coefficients estimated to b = 0, corresponding to regions without evidence for

the presence of two alleles at the SNPs considered. Sparsity in the coefficients and hence tolerance to false positive heterozygous SNPs due to sequencing error or ancient DNA damage was adjusted through the regularization parameter l.

A set of 1,107,975 bi-allelic reference SNPs polymorphic across the four high coverage archaic genomes (Altai, Chagyrskaya 8, Vindija 33.19, Denisova) and one human genome (HGDP01029, San) was first identified. For each target Neanderthal genome, the frequencies of the two alleles for each reference SNP covered by $\geq$ 2 reads in the target genome were then tabulated. The obtained vector of minor read allele frequencies along each chromosome was smoothed by fused lasso regression,[141] using the function 'fusedlasso1d' implemented in the *genlasso*[84] R package (version 1.6.1). To call ROHs, consecutive SNPs were collapsed with estimated coefficients $\beta < 0.005$ into segments. To test the feasibility of this approach to detect ROHs in low-coverage Neanderthal genomes, ROHs were called on simulated datasets of high-coverage genomes randomly down-sampled to lower coverage (2X and 1X). Lower values of the regularization parameter ($\lambda = 0.25$ or $\lambda = 0.5$) resulted in cumulative ROH lengths that were highly correlated between subsampled and full genomes (Figure S23). When using higher regularization (i.e., stronger emphasis on smoothing; $\lambda = 0.75$ or $\lambda = 1$), shorter segments tended to be missed in the subsampled genomes, resulting in a reduction of cumulative ROH length when using lower minimum ROH length (Figure S23). Conversely, cumulative ROH length at higher minimum length cutoffs were overestimated, due to merging of nearby shorter fragments (Figures S22, and S23). Both of these effects were particularly pronounced in the more challenging lowest coverage scenario (1X). Based on these results, we used a regularization parameter of $\lambda = 0.5$ in the final analyses.

Demographic modeling

We used the site-frequency spectrum (SFS)-based method *momi2*[54] to carry out demographic modeling from allele count data. Modeling was carried out using an SFS with ascertainment restricted to the four high-quality archaic samples with diploid genotypes (Altai Neanderthal, Chagyrskaya 8, Vindija 33.19, and Denisovan). To account for the exclusion of transition SNPs in the dataset, we used a transversion-only mutation rate of 0.16×10^{-9}/bp/year as estimated by Fu et al.[73] The generation time interval was assumed to be 29 years. Each demographic model was fit using ten independent replicates from randomized parameter starting values, to evaluate consistency of parameter estimates at convergence. We used the "TNC" method for model optimization, with a maximum number of 400 iterations. Confidence intervals for parameter estimates were obtained using 100 parametric bootstrap replicates, as implemented in the *momi2* package.

More specifically, a backbone demography was first fitted including only the high-coverage individuals, and incorporating previously inferred demographic events. The model included the following: (i) a shared archaic lineage ancestral to Denisovans and Neanderthals diverging from modern humans, (ii) early Siberian Neanderthals (represented by the Altai Neanderthal) diverging earliest within the Neanderthal clade, (iii) introgression of a "super-archaic" previously unsampled lineage into the Denisovan, and (iv) gene flow from the Altai Neanderthal into the Denisovan. We assumed a shared ancestral Neanderthal population size for the internal edges within the Neanderthal clade, and individual size parameters for each Neanderthal sample at the leaf. Previous studies have demonstrated low effective population sizes and evidence for recent inbreeding in Neanderthal populations,[8,15] population sizes at the leaf were therefore parameterized as exponentially decaying from their divergence to the sample age. Ten independent replicate fits were performed from random parameter starting values for this model to ensure convergence to a single optimum. The two low coverage samples Thorin and Mezmaiskaya 1 were then added to this initial model, as independent divergences from the Vindija 33.19 lineage and allowing it to occur at any time after its divergence from the Altai Neanderthal lineage. This new model was re-optimized in ten replicates, using the best fit parameter estimates from the initial model as starting values, and random initial values for the newly added demographic parameters (Figure 6, and Table S15).

To further investigate the relationship of the Forbes' Quarry Neanderthal with Thorin, we added FQ data to the previously obtained best-fit model and re-optimized using the same procedure as above. We considered two different scenarios for the divergence of FQ. In the first scenario, the FQ lineage was allowed to diverge from the Vindija lineage at any time between its initial divergence from the ancestor with the Altai Neanderthal. The best-fitting model for this scenario is presented Figure S25, left. In the second scenario, FQ was modeled to diverge from the Thorin lineage (Figure S25, right).

Additional models were performed to investigate the evidence for admixture with a deep Neanderthal lineage in the ~43 ka Les Cottés Z4-1514 sample from France (Figure S26). A new model was first fitted by adding the genomes of the late Neanderthals from Mezmaiskaya 2 and Les Cottés Z4-1514 to the best-fit model with Thorin described above. Based on the evidence from the D-statistic results, the Les Cottés Z4-1514 lineage was modeled as a mixture of a late European Vindija-like lineage (constrained to diverge after Mezmaiskaya 2), and an early European lineage (constrained to diverge prior to Mezmaiskaya 2). The resulting model is presented (Figure S26, left). To test whether this model fit significantly better than a model without admixture, a nested model was fit with the same configuration but the admixture proportion constrained to zero (Figure S26, middle). To further investigate whether the "deep" European Neanderthal contribution in Les Cottés Z4-1514 observed (Figure S26, middle) was related to Thorin, another model was fit, where the deep lineage was allowed to only diverge from the Thorin lineage (Figure S26, right).